

# Experimental Phase Equilibria Studies in the FeO-Fe<sub>2</sub>O<sub>3</sub>-CaO-SiO<sub>2</sub> System and the Subsystems CaO-SiO<sub>2</sub>, FeO-Fe<sub>2</sub>O<sub>3</sub>-SiO<sub>2</sub> in Air



SIYU CHENG , MAKSYM SHEVCHENKO , PETER C. HAYES ,  
and EVGUENI JAK

New experimental measurements have been made to determine liquidus isotherms, univariant and invariant equilibria in the FeO-Fe<sub>2</sub>O<sub>3</sub>-CaO-SiO<sub>2</sub>, CaO-SiO<sub>2</sub> and FeO-Fe<sub>2</sub>O<sub>3</sub>-SiO<sub>2</sub> systems in air at temperatures between 1190 °C and 1730 °C. The study was undertaken using equilibration/quenching and microanalysis techniques, enabling the compositions of the liquid and solid phases in equilibrium at temperature to be accurately measured. The data have been used to define liquidus in the primary phase fields of hematite (Fe<sub>2</sub>O<sub>3</sub>), spinel [(Fe,Ca)O·Fe<sub>2</sub>O<sub>3</sub>], lime (CaO), tridymite or cristobalite (SiO<sub>2</sub>), dicalcium ferrite (2CaO·Fe<sub>2</sub>O<sub>3</sub>, C<sub>2</sub>F), pseudo-wollastonite (CaO·SiO<sub>2</sub>, CS), rankinite (3CaO·2SiO<sub>2</sub>, C<sub>3</sub>S<sub>2</sub>), dicalcium silicate (2CaO·SiO<sub>2</sub>, C<sub>2</sub>S), tricalcium silicate (3CaO·SiO<sub>2</sub>, C<sub>3</sub>S) and the two liquids miscibility gap. These data obtained in the present study provide a more complete and more accurate description of the multi-component Fe-Ca-Si-O-Al-Mg-Cu-S system directly relevant to applications in the cement, the ferrous and non-ferrous metallurgical industries.

<https://doi.org/10.1007/s11663-021-02159-w>

© The Minerals, Metals & Materials Society and ASM International 2021

## I. INTRODUCTION

THE FeO-Fe<sub>2</sub>O<sub>3</sub>-CaO-SiO<sub>2</sub> system forms the basis for understanding the chemical behavior of slags and compounds that are encountered in a wide range of metallurgical ferrous and non-ferrous industrial processes. For example, the iron-rich silica-poor region of the system in oxidizing conditions is particularly important to iron ore sintering and pelletizing. Regions with intermediate silica concentrations are of particular interests for the non-ferrous smelting processes in intermediate reducing conditions ( $pO_2 = 10^{-6}$  to  $10^{-8}$ ). The calcium silicate primary phase fields are important for the steelmaking, refractory and cement manufacture. The characterization of phase equilibria in this system is crucial to understanding the reaction paths taken during these processes, and to the selection of appropriate fluxing and blending strategies.

The silico-ferrite of calcium and aluminum solid solution (SFCA, where S, F, C and A indicate SiO<sub>2</sub>, Fe<sub>2</sub>O<sub>3</sub>, CaO and Al<sub>2</sub>O<sub>3</sub> respectively, although oxidation state of Fe can be variable in this phase or group of closely related phases) is a key phase in the iron ore sintering process as it constitutes a large proportion of materials present in the industrial sinter products and is believed to enhance the reducibility and mechanical strength of the sinters. This phase is limited by the silico-ferrite of calcium (SFC) solid solution in the “Fe<sub>2</sub>O<sub>3</sub>”-CaO-SiO<sub>2</sub> system. Previous works on the phase equilibria in this system have been carried out by the authors in the iron-rich region in air,<sup>[1,2]</sup> and in 1 atm CO<sub>2</sub>.<sup>[3]</sup> The effect of Al<sub>2</sub>O<sub>3</sub> have also been investigated in later studies by the authors.<sup>[4,5]</sup> These studies have provided firm understandings of phase equilibria in certain compositional regions, although there are still lack of reliable experimental data in different systems. The present study focuses on the regions where no previous data is available in the “Fe<sub>2</sub>O<sub>3</sub>”-CaO-SiO<sub>2</sub> system in air.

Measurements of the liquidus temperatures and the compositions of the solid phases formed in the CaO-SiO<sub>2</sub> system in air have been reported in previous publications.<sup>[6-17]</sup> A critical thermodynamic assessment of the CaO-SiO<sub>2</sub> system was carried out by Eriksson *et al.*<sup>[18]</sup> incorporating the experimental work by a number of authors.<sup>[6,8,14-16]</sup> There remain some uncertainties in the data and differences in the thermodynamic

SIYU CHENG, MAKSYM SHEVCHENKO, PETER C. HAYES, and EVGUENI JAK are with the PYROSEARCH, Pyrometallurgy Innovation Centre, School of Chemical Engineering, The University of Queensland, Brisbane, QLD 4072, Australia. Contact e-mail: s.cheng@uq.edu.au

Manuscript submitted July 21, 2020; accepted March 24, 2021.

Article published online April 13, 2021.

descriptions of this system, in particular, (i) the solubilities of CaO and SiO<sub>2</sub> in CaO·SiO<sub>2</sub><sup>[6]</sup>; (ii) the solubility of CaO in 2CaO·SiO<sub>2</sub><sup>[8]</sup>; (iii) the low temperature limit of 3CaO·SiO<sub>2</sub> stability—temperature of formation from CaO and α'-2CaO·SiO<sub>2</sub><sup>[6,8,10]</sup>; and (iv) the high temperature limit of stability of 3CaO·SiO<sub>2</sub>—whether 3CaO·SiO<sub>2</sub> decomposes to CaO and α-2CaO·SiO<sub>2</sub> at sub-liquidus,<sup>[6,8]</sup> or is stable up to the liquidus in the CaO·SiO<sub>2</sub> system.<sup>[11,12]</sup>

The liquidus temperatures in the FeO-Fe<sub>2</sub>O<sub>3</sub>-SiO<sub>2</sub> system in air have been previously experimentally investigated,<sup>[14,15,19,20]</sup> and thermodynamic optimizations of the system presented by a number of researchers.<sup>[21–24]</sup> There are differences in the reported values of the eutectic temperature and the composition of the eutectic in this system. In addition, Liu<sup>[20]</sup> using Electron Probe X-ray Microanalysis (EPMA) reported 1.5 wt pct Fe<sub>2</sub>O<sub>3</sub> in solid solution in cristobalite. In an independent study by Kawasaki,<sup>[25]</sup> approximately 0.75 wt pct of the apparent solubility of “Fe<sub>2</sub>O<sub>3</sub>” in SiO<sub>2</sub> was considered to be a result from the secondary fluorescence associated with the EPMA measurement rather than a true chemical solubility (0.25 wt pct).

The FeO-Fe<sub>2</sub>O<sub>3</sub>-CaO system in air has been investigated experimentally<sup>[20,26,27]</sup> and thermodynamically optimized,<sup>[28,29]</sup> and then further revised experimentally by the authors<sup>[30]</sup> with the focus on the invariant points between liquid-2CaO·Fe<sub>2</sub>O<sub>3</sub>-CaO·Fe<sub>2</sub>O<sub>3</sub>, liquid-CaO·Fe<sub>2</sub>O<sub>3</sub>-CaO·2Fe<sub>2</sub>O<sub>3</sub>, and liquid-CaO·2Fe<sub>2</sub>O<sub>3</sub>-hematite. The later experimental investigation of this system<sup>[30]</sup> provided additional information on the locations of the liquidus and invariant points.

The experimental data on the liquidus surface of the “Fe<sub>2</sub>O<sub>3</sub>”-CaO-SiO<sub>2</sub> pseudo-ternary system in air are available on: the calcium-rich region,<sup>[31]</sup> extensive regions below 50 wt pct SiO<sub>2</sub>,<sup>[32]</sup> the 1300 °C isotherm,<sup>[33]</sup> the hematite-tridymite and the spinel-tridymite univariant lines,<sup>[24,33]</sup> and the iron-rich region with the focus on the SFC (Silico-Ferrite of Calcium) solid solution.<sup>[1,2,34,35]</sup> These equilibrium data were obtained using various characterization methods including: (i) optical microscopy and wet chemical analysis,<sup>[31,32]</sup> (ii) X-ray Powder Diffraction (XRD)<sup>[34,35]</sup> and (iii) EPMA.<sup>[1,2,24,33–35]</sup> The extent of the 3CaO·SiO<sub>2</sub> primary phase field has not been fully defined. There are inconsistencies on the 3CaO·SiO<sub>2</sub> primary phase field extending up to the CaO-SiO<sub>2</sub> binary,<sup>[32]</sup> or only up to 26.6 wt pct Fe<sub>2</sub>O<sub>3</sub> in the pseudo-ternary system.<sup>[31]</sup> In recent phase equilibria studies on the CaO-ZnO-SiO<sub>2</sub><sup>[36]</sup> and CaO-PbO-SiO<sub>2</sub><sup>[37]</sup> systems, an upper temperature stability limit of C<sub>3</sub>S above 1900 °C was estimated, supporting the data by some of the previous authors.<sup>[11,12]</sup> Additionally, no equilibrium data are available in the regions above 50 wt pct SiO<sub>2</sub> on the cristobalite liquidus surface and in the regions of the two liquid miscibility gap. The most recent thermodynamic assessment of this system was carried out by Hidayat *et al.*<sup>[38]</sup>

To summarize, to date there is a lack of reliable phase equilibria experimental data in the “Fe<sub>2</sub>O<sub>3</sub>”-CaO-SiO<sub>2</sub> system in air, particularly at high temperatures. The aim of the present study is to develop a full and systematic

experimental characterization of: (i) the liquidus surface on the “Fe<sub>2</sub>O<sub>3</sub>”-CaO-SiO<sub>2</sub> system in air, and (ii) the sub-systems CaO-SiO<sub>2</sub> and “Fe<sub>2</sub>O<sub>3</sub>”-SiO<sub>2</sub> in air up to 1730 °C where no experimental data are available at high temperatures using quantitative microanalysis techniques. The accuracies of the data are improved in the present study by minimizing uncertainties from quenching high temperature slags and from the measurements (as described in detail in next section). This will provide accurate data in support of development of thermodynamic models of the higher order systems that are encountered in a wide range of industrial applications.

## II. EXPERIMENTAL METHODOLOGY

The equilibration/quenching/EPMA measurement approach used in the present study, developed by the authors,<sup>[39,40]</sup> has been described in detail in previous publications.<sup>[1,2,36,37]</sup>

Initial mixtures used in the present study were made by mixing, (i) high-purity powders of Fe<sub>2</sub>O<sub>3</sub> (99.9 wt pct), CaCO<sub>3</sub> (99.9 wt pct), SiO<sub>2</sub> (99.9 wt pct) supplied by Sigma-Aldrich Co, NSW, Australia, and (ii) a pre-melted CaO-SiO<sub>2</sub> master slag (the eutectic at 61 mol pct SiO<sub>2</sub>). SiO<sub>2</sub> powder was pre-heated at 400 °C in air in a muffle furnace for at least 4 hours to remove moisture, and immediately used for mixture preparation. The use of the master slag was found to be advantageous in that it: (i) further minimized moisture absorption on the surfaces of the fine SiO<sub>2</sub> powder and improved the accuracy of the mixture starting compositions, (ii) facilitated chemical reactions between components at lower temperature, since higher density mixtures were obtained, and (iii) enhanced the homogeneity of the samples. Consequently, all initial mixtures were prepared from either (CaCO<sub>3</sub> + master-slag + Fe<sub>2</sub>O<sub>3</sub>) or (master-slag + SiO<sub>2</sub> + Fe<sub>2</sub>O<sub>3</sub>) powders.

In each equilibration experiment less than 0.3 g of the mixture was used. Each of the mixtures were pressed into pellet using a tool steel die. The initial compositions of the mixtures were selected so that, at the equilibration temperature, one or more crystalline phases would be present in equilibrium with liquid slag. The sample composition was selected so that the volume fraction of solids was targeted to be below 50 pct, and preferably approximately 10 pct, to achieve rapid equilibration and useful outcomes from quenching. It was found that the solids serve as heterogeneous nucleation centers, and the minimum distance between them should exceed 10–20 μm to ensure that amorphous slag of uniform composition, unaffected by microcrystal growth, is obtained. The optimum fraction of solids was found to be dependent on the slag composition and the equilibrium temperature; these factors influence the slag viscosity, and equilibration time, and the kinetics of crystallization of the melt on cooling. An iterative procedure involving preliminary experiments was often needed to achieve the targeted proportions of the phases for a given final

**Table I. Average Apparent Solubility Wt Pct of B Observed in Solid A (Pre-sintered, 50-100  $\mu\text{m}$ ) Due to Secondary X-ray Fluorescence Associated with EPMA Measurement of the A Phase,  $\text{C}_2\text{F} = \text{Ca}_2\text{Fe}_2\text{O}_5$ ,  $\text{CF} = \text{CaFe}_2\text{O}_4$ ,  $\text{CS} = \text{CaSiO}_3$ ,  $\text{C}_3\text{S}_2 = \text{Ca}_3\text{Si}_2\text{O}_7$**

| Solid B Matrix<br>(Fine Powder)                            | $\text{Fe}_2\text{O}_3$ | $\text{CaO}$ | $\text{SiO}_2$ |
|--|-------------------------|--------------|----------------|
| Solid A particles<br>(pre-sintered, 50-100 $\mu\text{m}$ ) |                         |              |                |
| $\text{Fe}_2\text{O}_3$                                    | —                       | —            | 0.0            |
| $\text{Fe}_3\text{O}_4$                                    | —                       | 0.0          | —              |
| $\text{CaO}$   | 1.3                     | —            | —              |
| $\text{SiO}_2$   | 1.1                     | —            | —              |
| $\text{C}_2\text{F}$ - $\text{CF}$ mixture                 | —                       | —            | 0.0            |
| $\text{CS}$ - $\text{C}_3\text{S}_2$ mixture               | 0.7                     | —            | —              |

**Table II. Different Starting Compositions Selected to Approach Equilibrium From Different Directions**

| Initial Mixture ID  | Starting Mixtures (Wt Pct)       |                   |                  |                                |                     | Mol Pct |                       |                  |
|---|----------------------------------|-------------------|------------------|--------------------------------|---------------------|---------|-----------------------|------------------|
|   | CaO-SiO <sub>2</sub> Master Slag | CaCO <sub>3</sub> | SiO <sub>2</sub> | Fe <sub>2</sub> O <sub>3</sub> | Fe <sub>1-y</sub> O | CaO     | “FeO <sub>1.5</sub> ” | SiO <sub>2</sub> |
| a. Equilibrate from Mixtures in Different Primary Phase Fields          |                                  |                   |                  |                                |                     |         |                       |                  |
| A   | 58.7                             | 0.0               | 0.0              | 41.3                           | 0.0                 | 25.6    | 34.4                  | 40.0             |
| B   | 69.8                             | 4.4               | 0.0              | 25.8                           | 0.0                 | 32.5    | 21.0                  | 46.5             |
| b. Equilibrate from Mixtures with Different Total Oxygen Concentrations |                                  |                   |                  |                                |                     |         |                       |                  |
| C   | 16.4                             | 0.0               | 58.1             | 0.0                            | 25.5                | 7.0     | 22.0                  | 71.0             |
| D   | 15.9                             | 0.0               | 56.7             | 27.4                           | 0.0                 | 7.0     | 22.0                  | 71.0             |

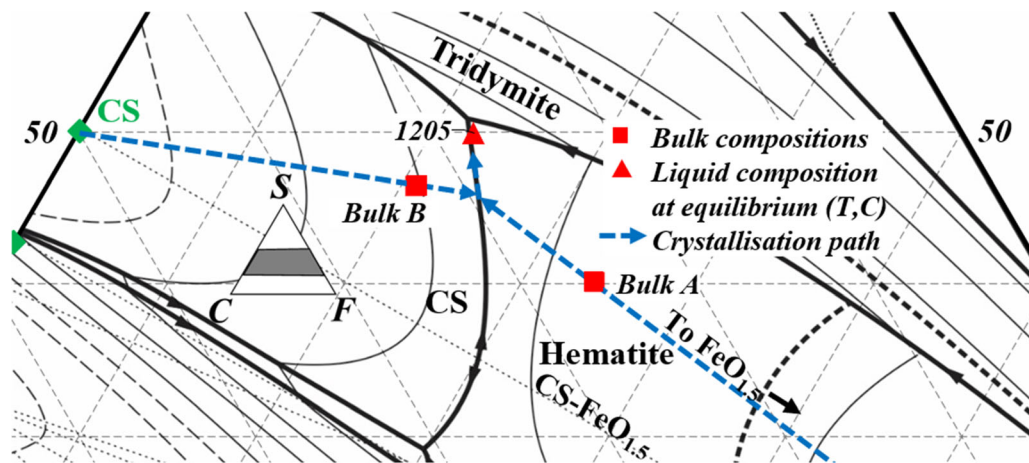


Fig. 1—Equilibrium approached from two starting compositions (Bulk A, B) selected in different primary phase fields in the “FeO<sub>1.5</sub>”-CaO-SiO<sub>2</sub> system in air and equilibrated at the same temperature (1205 °C). Compositions in mol pct, CS = Pseudo-wollastonite.

**Table III. Results of Measured Compositions of Liquid(s) Equilibrating from Different Directions at the Same Temperatures**

| Initial Mixture ID | Temperature, °C | Measured Liquid Compositions, Mol Pct |                       |                  |      |                       |                  |
|--------------------|-----------------|---------------------------------------|-----------------------|------------------|------|-----------------------|------------------|
|                    |                 | Liq1                                  |                       |                  | Liq2 |                       |                  |
|                    |                 | CaO                                   | “FeO <sub>1.5</sub> ” | SiO <sub>2</sub> | CaO  | “FeO <sub>1.5</sub> ” | SiO <sub>2</sub> |
| A                  | 1205            | 27.6                                  | 22.5                  | 49.9             | —    | —                     | —                |
| B                  | 1205            | 27.3                                  | 22.7                  | 50.0             | —    | —                     | —                |
| C                  | 1683            | 8.3                                   | 26.2                  | 65.5             | 1.2  | 4.0                   | 94.8             |
| D                  | 1683            | 8.5                                   | 26.0                  | 65.5             | 1.3  | 4.1                   | 94.6             |

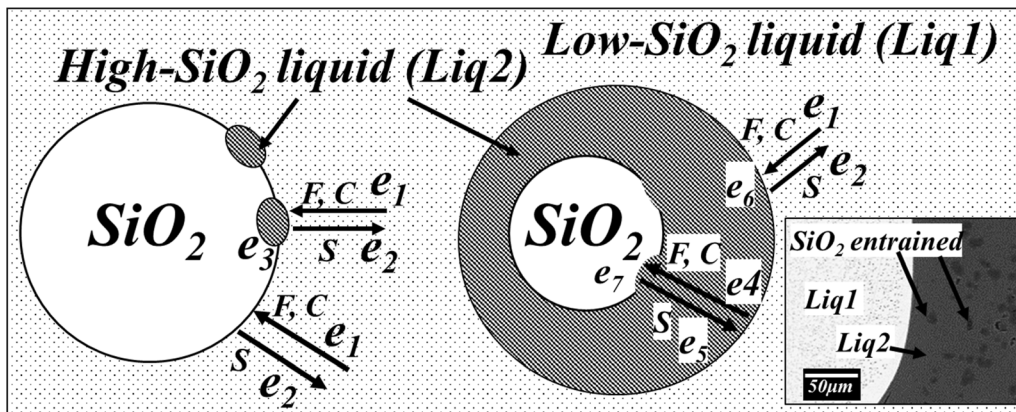


Fig. 2—Schematic diagram showing reaction steps of formation of high-SiO<sub>2</sub> liquid on the interface between Cristobalite (SiO<sub>2</sub>) and low-SiO<sub>2</sub> liquid resulting in metastable entrained SiO<sub>2</sub> in the high-SiO<sub>2</sub> liquid, F = Fe<sup>2+</sup>, Fe<sup>3+</sup>; C = Ca<sup>2+</sup> and S = Si<sup>4+</sup>.

temperature and composition, since the exact liquidus temperatures at given compositions were not initially known.

Three types of substrates were used for supporting the samples during equilibration, (i) a platinum wire spiral, (ii) a platinum foil envelope (specifications and reasons for selections have been described in detail in a previous publication<sup>[2]</sup>), and (iii) an open cylindrical SiO<sub>2</sub> crucible (Outer Dia. 18 mm\*Inner Dia. 15 mm\*Length 12 mm, supplied by Lianyungang Guoyi Quartz Products Co., Ltd, Jiangsu, China) for containing slags in equilibrium with tridymite and cristobalite.

All equilibration experiments were carried out in a vertical reaction tube (impervious recrystallized alumina, 30-mm inner diameter) within an electrical resistance lanthanum chromite heated furnace. The samples were placed immediately adjacent to a working thermocouple in a recrystallized alumina sheath in the uniform hot zone of the furnace to monitor the actual sample temperature. The working thermocouple (100 pct Pt/87 pct Pt-13 pct Rh) was calibrated against a standard thermocouple (supplied by the National Measurement Institute of Australia, NSW, Australia). The overall absolute temperature accuracy of each experiment was estimated to be  $\pm 3$  K. The bottom of the furnace was open to ensure ambient air atmosphere inside,  $p(\text{O}_2) = 0.21$  atm.

The samples were suspended in the hot zone of the furnace by Kanthal support wire (Fe-Cr-Al alloy, 0.7 mm diameter). For temperatures higher than 1450 °C, a 0.5 mm diameter pure Pt wire was used to extend the support so that the Kanthal wire is not in the hot zone. The samples were pre-melted for 15-30 minutes at temperatures 5-100 °C above the equilibration temperature, to facilitate the formation of a homogeneous liquid slag. Some samples were then pre-cooled for another 15-30 minutes at temperatures 5-20 °C below the equilibration temperature, followed by equilibration at the final target temperature for the required time. The pre-melt and pre-cool procedures are designed to confirm the achievement of equilibrium from different thermal trajectories. At the end of the equilibration

process, the samples were released and rapidly quenched into CaCl<sub>2</sub>-containing brine (< 253 K (- 20 °C)). The samples were then washed thoroughly in water and ethanol before being dried on a hot plate, and mounted in epoxy resin. Polished cross-sections were prepared using conventional metallographic techniques. CaO- and 2CaO·SiO<sub>2</sub>-containing samples were polished in kerosene to avoid hydrations.

The samples were first examined by optical microscopy, then carbon-coated and the phase compositions were measured using an electron probe X-ray microanalysis technique with wavelength dispersive detectors (JEOL 8200L EPMA, Japan Electron Optics Ltd., Tokyo, Japan). In the present study, the EPMA is operated at 15 kV accelerating voltage and 20 nA probe current using the standard Duncumb-Philibert atomic number, absorption, and fluorescence (ZAF) correction supplied by JEOL.<sup>[41-43]</sup> The standards used (supplied by Charles M. Taylor Co., Stanford, CA) include: wollastonite (CaSiO<sub>3</sub>) for calcium (K $\alpha$ ) and silica (K $\alpha$ ) calibration, hematite (Fe<sub>2</sub>O<sub>3</sub>) for iron (K $\alpha$ ) calibration, and in some cases alumina (K $\alpha$ ) (Al<sub>2</sub>O<sub>3</sub>) and platinum (L $\alpha$  or M $\alpha$ ) (Pt) to test for possible contamination. Fe is always present in the slag in two oxidation states Fe<sup>2+</sup> and Fe<sup>3+</sup>. Only the concentrations of the metal cations were measured by EPMA in the present study. All cation concentrations measured with EPMA were then recalculated to selected oxidation states (*i.e.* FeO<sub>1.5</sub>, SiO<sub>2</sub> and CaO) and normalized to 100 pct for presentation purposes only. The normalized phase compositions and original sums of elements or oxides from the EPMA analyses are provided in tabular form. The total compositions before normalization to 100 pct are also reported in Table V, indicated as “old total”.

The ability to quench the liquid slag phase to ambient temperature without the onset of crystallization was found to depend on the composition of the slag and the equilibration temperature. The most significant problems were observed with low-SiO<sub>2</sub> slags at high temperatures, at or above 1300 °C, where the glassy homogeneous areas were only a small proportion of the melt, believed to be formed at the surfaces directly

Table IV. Descriptions of Reaction Occurring During Formation of the High-SiO<sub>2</sub> Liquid

| Steps          | Descriptions  |
|----------------|---|
| e <sub>1</sub> | diffusion of Ca <sup>2+</sup> , Fe <sup>2+</sup> , Fe <sup>3+</sup> from bulk Liq1 to Liq1-SiO <sub>2</sub> or Liq1-Liq2 interface  |
| e <sub>2</sub> | Si <sup>4+</sup> counter-diffusion from Liq1-SiO <sub>2</sub> or Liq1-Liq2 interface to bulk Liq1   |
| e <sub>3</sub> | reaction between Ca <sup>2+</sup> , Fe <sup>2+</sup> , Fe <sup>3+</sup> and Si <sup>4+</sup> at Liq1-SiO <sub>2</sub> interface forming Liq2<br>[(Ca <sup>2+</sup> , Fe <sup>2+</sup> , Fe <sup>3+</sup> ) <sub>liq1</sub> + Si <sup>4+</sup> <sub>SiO2</sub> → Liq2] |
| e <sub>4</sub> | diffusion of Ca <sup>2+</sup> , Fe <sup>2+</sup> , Fe <sup>3+</sup> through the newly formed Liq2 from Liq2 to Liq2-SiO <sub>2</sub> interface  |
| e <sub>5</sub> | diffusion of Si <sup>4+</sup> through the newly formed Liq2 from SiO <sub>2</sub> to Liq1-Liq2 interface  |
| e <sub>6</sub> | reaction between Ca <sup>2+</sup> , Fe <sup>2+</sup> , Fe <sup>3+</sup> and Si <sup>4+</sup> at Liq1-Liq2 interface forming Liq2<br>[(Ca <sup>2+</sup> , Fe <sup>2+</sup> , Fe <sup>3+</sup> ) <sub>liq1</sub> + Si <sup>4+</sup> <sub>Liq2</sub> → Liq2]             |
| e <sub>7</sub> | reaction between Ca <sup>2+</sup> , Fe <sup>2+</sup> , Fe <sup>3+</sup> and Si <sup>4+</sup> at Liq2-SiO <sub>2</sub> interface forming Liq2<br>[(Ca <sup>2+</sup> , Fe <sup>2+</sup> , Fe <sup>3+</sup> ) <sub>liq2</sub> + Si <sup>4+</sup> <sub>SiO2</sub> → Liq2] |

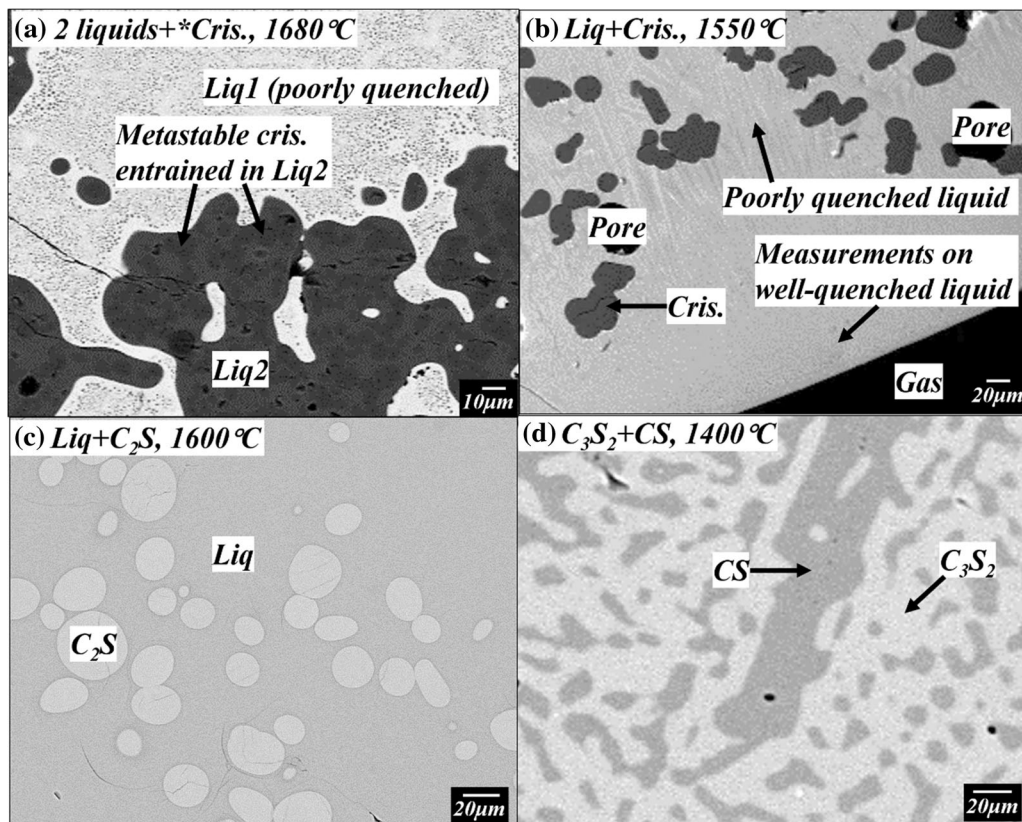


Fig. 3—Backscattered images taken on JEOL 8200L showing typical microstructure of samples in the “FeO<sub>1.5</sub>”-SiO<sub>2</sub> pseudo-binary system in air and the CaO-SiO<sub>2</sub> binary system in air, corresponding experiment number = exp. (a) 2 liquids + metastable cristobalite surrounded by high viscosity of SiO<sub>2</sub>-rich liquid, exp. 8, (b) Liq. + cristobalite, exp.5, (c) Liq. + C<sub>2</sub>S, exp.12, (d) C<sub>3</sub>S<sub>2</sub> + CS, exp.19.

contacting the quenching medium. For these samples the approach taken to obtain accurate, repeatable, and objective measurements of the average compositions of the liquid slag phase by the use of EPMA was similar to that described by Nikolic *et al.*<sup>[44]</sup>: an average of at least 20 points in the best quenched area (usually, near the surface) was used, with a standard deviation of composition not exceeding 1 mol pct. In cases where melt crystallization was rapid, the experiments were repeated until a sufficient area of the well-quenched

microstructure was found. Increasing the probe diameter to 5-50 μm resulted in reduced variability of the measured liquid slag compositions.<sup>[45]</sup>

The standard ZAF correction was further improved following the same approach as described in detail in previous publications.<sup>[1,2]</sup> Using stoichiometric Fe<sub>2</sub>SiO<sub>4</sub>, Ca<sub>2</sub>Fe<sub>2</sub>O<sub>5</sub>, CaFe<sub>2</sub>O<sub>4</sub> and CaFe<sub>4</sub>O<sub>7</sub> as secondary standards, an analytical expression is developed to correct all cation concentrations in the “FeO<sub>1.5</sub>”-CaO-SiO<sub>2</sub> system:

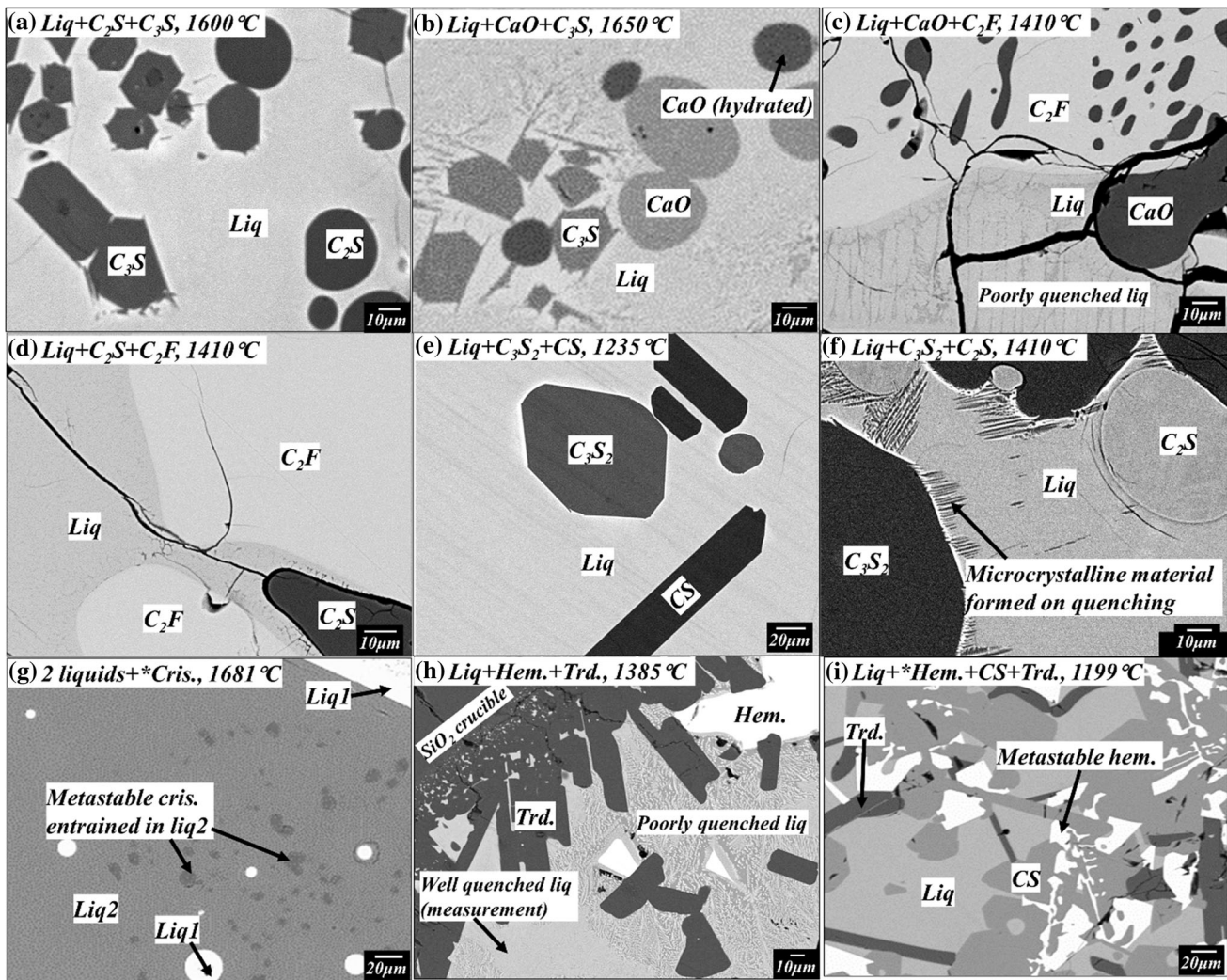


Fig. 4—Backscattered images taken on JEOL 8200L showing typical microstructure of samples in the “FeO<sub>1.5</sub>”-CaO-SiO<sub>2</sub> pseudo-ternary system in air, (a) Liq + C<sub>2</sub>S + C<sub>3</sub>S, exp.111, (b) Liq + CaO + C<sub>3</sub>S, exp.104, (c) Liq + CaO + C<sub>2</sub>F, exp.102, (d) Liq + C<sub>2</sub>S + C<sub>2</sub>F, exp.99, (e) Liq + C<sub>3</sub>S<sub>2</sub> + CS, exp.89, (f) Liq + C<sub>3</sub>S<sub>2</sub> + C<sub>2</sub>S, exp.92, (g) 2 liquids + metastable cristobalite entrained in high viscosity of SiO<sub>2</sub>-rich liquid, exp.122, (h) Liq + hematite + tridymite, exp.76, (i) Liq + CS + tridymite + metastable hematite, exp.124. \*One of the phases is metastable because of: (i) minor impurity (< 0.1 mol pct); or (ii) local temperature fluctuation due to furnace control.

$$x(\text{SiO}_2)^{\text{corr}} = x(\text{SiO}_2) - 0.0637x(\text{SiO}_2)x(\text{FeO}_{1.5})(1 - x(\text{SiO}_2))$$

$$x(\text{CaO})^{\text{corr}} = x(\text{CaO}) - x(\text{CaO})x(\text{FeO}_{1.5})(0.0208 + 0.0119(x(\text{FeO}_{1.5}) - x(\text{CaO})))$$

$$x(\text{FeO}_{1.5})^{\text{corr}} = 1 - x(\text{SiO}_2)^{\text{corr}} - x(\text{CaO})^{\text{corr}}$$

where  $x(\text{SiO}_2, \text{CaO}, \text{FeO}_{1.5})$  are the cation molar fractions following JEOL ZAF correction,  $x(\text{SiO}_2, \text{CaO}, \text{FeO}_{1.5})^{\text{corr}}$  are the corrected cation molar fractions.

The overestimation of concentrations of some elements such as Fe, Cu, Zn measured with EPMA in tridymite or cristobalite (SiO<sub>2</sub>), lime (CaO), and different calcium silicates (Ca<sub>x</sub>Si<sub>y</sub>O<sub>z</sub>) present within the Fe, Cu, Zn containing matrix (slag) attributed to the secondary fluorescence by the X-rays originated from the continuum background spectra of the braking electrons (bremsstrahlung) was previously reported.<sup>[46,47]</sup> Same effect was observed by the present authors in previous studies (Fe,<sup>[48,49]</sup> Cu,<sup>[50,51]</sup> Zn<sup>[49,51,52]</sup>

measured in tridymite and cristobalite (SiO<sub>2</sub>)). This effect was only detected for the measurements using characteristic X-ray lines with energies above 5 keV; the X-rays from the continuum background with these energies have high (> 100 micron) penetration ability through the SiO<sub>2</sub> or other particles of comparable density into the surrounding matrix (e.g. slag) thus exciting the characteristic lines of Fe, Cu, Zn in the matrix and therefore generating the incorrect apparent overestimated values of concentrations of these elements in such particles.<sup>[46,47]</sup> This is proven by a series of special experiments undertaken in the present study, by preparing a pelletized mixture of pre-sintered solids (A) with grains of 10-100 μm diameter with fine powder of solids (B) matrix. In this mixture the proportions of the phases were selected such that the individual “A” grains were surrounded by pure solid “B” matrix. The results of microanalysis of the “A” phases are listed in Table I. The secondary fluorescence of the Fe<sub>2</sub>O<sub>3</sub> detected on

**Table V. Molar Compositions and Standard Deviations of the Phases Measured by EPMA in the “FeO<sub>1.5</sub>”- SiO<sub>2</sub>, CaO-SiO<sub>2</sub> and “FeO<sub>1.5</sub>”-CaO-SiO<sub>2</sub> System in Air**

| No.  | Temp., °C | Time, h | Phase Assemblages  | Composition (mol pct) |              |                    |              |                  |              | “Old (Wt Pct)” | Total” |
|--|-----------|---------|--|-----------------------|--------------|--------------------|--------------|------------------|--------------|----------------|--------|
|  |           |         |  | CaO                   | St. Dev.     | FeO <sub>1.5</sub> | St. Dev.     | SiO <sub>2</sub> | St. Dev.     |                |        |
| <i>“FeO<sub>1.5</sub>”-SiO<sub>2</sub> system in air</i> |           |         |  |                       |              |                    |              |                  |              |                |        |
| Spinel ppf.  |           |         |  |                       |              |                    |              |                  |              |                |        |
| 1  | 1500      | 4       | liq<br>spinel  | 0.0<br>0.0            | 0.00<br>0.00 | 87.5<br>99.9       | 0.11<br>0.01 | 12.5<br>0.1      | 0.09<br>0.02 | 103.7<br>104.3 |        |
| Cristobalite ppf.  |           |         |  |                       |              |                    |              |                  |              |                |        |
| 2  | 1670      | 1       | liq<br>cristobalite  | 0.0<br>0.0            | 0.02<br>0.00 | 61.9<br>0.7        | 0.21<br>0.10 | 38.0<br>99.3     | 0.21<br>0.13 | 104.0<br>101.7 |        |
| 3  | 1650      | 1       | liq<br>cristobalite  | 0.0<br>0.0            | 0.00<br>0.00 | 63.7<br>0.6        | 0.22<br>0.27 | 36.3<br>99.4     | 0.22<br>0.28 | 103.4<br>101.4 |        |
| 4  | 1600      | 2       | liq<br>cristobalite  | 0.0<br>0.0            | 0.00<br>0.00 | 69.9<br>0.4        | 0.22<br>0.09 | 30.1<br>99.6     | 0.22<br>0.09 | 103.7<br>101.8 |        |
| 5  | 1550      | 4       | liq<br>cristobalite  | 0.0<br>0.0            | 0.00<br>0.00 | 73.9<br>0.4        | 0.14<br>0.07 | 26.0<br>99.6     | 0.13<br>0.07 | 104.2<br>101.5 |        |
| 6  | 1500      | 4       | liq<br>cristobalite  | 0.0<br>0.0            | 0.00<br>0.00 | 78.6<br>0.3        | 0.28<br>0.04 | 21.4<br>99.7     | 0.04<br>0.26 | 103.5<br>101.1 |        |
| Two immiscible liquids                                   |           |         |  |                       |              |                    |              |                  |              |                |        |
| 7  | 1730      | 0.5     | liq1<br>liq2   | 0.0<br>0.0            | 0.00<br>0.00 | 55.7<br>3.9        | 0.80<br>0.16 | 44.3<br>96.1     | 0.80<br>0.16 | 104.6<br>101.0 |        |
| 8  | 1680      | 1       | liq1<br>liq2   | 0.0<br>0.0            | 0.00<br>0.00 | 60.9<br>2.4        | 0.33<br>0.10 | 39.1<br>97.5     | 0.32<br>0.10 | 105.3<br>101.2 |        |
| <i>CaO-SiO<sub>2</sub> system in air</i>                 |           |         |  |                       |              |                    |              |                  |              |                |        |
| Pseudo-wollastonite (CS) ppf.                            |           |         |  |                       |              |                    |              |                  |              |                |        |
| 9  | 1470      | 24      | liq<br>cs  | 56.0<br>50.0          | 0.11<br>0.04 | 0.0<br>0.0         | 0.00<br>0.00 | 44.0<br>50.0     | 0.11<br>0.04 | 100.4<br>100.5 |        |
| 10   | 1450      | 24      | liq<br>cs  | 38.8<br>50.1          | 0.13<br>0.08 | 0.0<br>0.0         | 0.00<br>0.00 | 61.2<br>49.9     | 0.13<br>0.08 | 99.0<br>99.6   |        |
| Dicalcium Silicate (C <sub>2</sub> S) ppf.               |           |         |  |                       |              |                    |              |                  |              |                |        |
| 11   | 1730      | 0.5     | liq<br>$\alpha$ -C <sub>2</sub> S                            | 59.1<br>66.8          | 0.10<br>0.09 | 0.0<br>0.0         | 0.00<br>0.00 | 40.9<br>33.2     | 0.10<br>0.09 | 99.9<br>98.9   |        |
| 12   | 1600      | 2       | liq<br>$\alpha$ -C <sub>2</sub> S                            | 57.7<br>66.6          | 0.11<br>0.16 | 0.0<br>0.0         | 0.00<br>0.00 | 42.2<br>33.4     | 0.12<br>0.16 | 99.9<br>100.5  |        |
| 13   | 1500      | 4       | liq<br>$\alpha$ -C <sub>2</sub> S                            | 56.8<br>66.7          | 0.08<br>0.10 | 0.0<br>0.0         | 0.00<br>0.02 | 43.1<br>33.3     | 0.09<br>0.09 | 99.8<br>100.3  |        |
| Cristobalite ppf.  |           |         |  |                       |              |                    |              |                  |              |                |        |
| 14   | 1650      | 2       | liq<br>cristobalite  | 30.9<br>0.6           | 0.07<br>0.16 | 0.0<br>0.0         | 0.04<br>0.00 | 69.0<br>99.4     | 0.06<br>0.17 | 99.5<br>99.3   |        |
| Tridymite ppf.   |           |         |  |                       |              |                    |              |                  |              |                |        |
| 15   | 1450      | 24      | liq<br>tridymite   | 36.9<br>0.1           | 0.08<br>0.03 | 0.0<br>0.0         | 0.00<br>0.00 | 63.1<br>99.9     | 0.08<br>0.04 | 99.0<br>100.5  |        |
| Two immiscible liquids                                   |           |         |  |                       |              |                    |              |                  |              |                |        |
| 16   | 1730      | 0.5     | liq1<br>liq2   | 25.5<br>1.4           | 0.15<br>0.07 | 0.0<br>0.0         | 0.00<br>0.00 | 74.5<br>98.6     | 0.14<br>0.08 | 99.4<br>99.5   |        |
| 17   | 1700      | 1       | liq1<br>liq2   | 26.4<br>1.1           | 0.12<br>0.07 | 0.0<br>0.0         | 0.00<br>0.00 | 73.6<br>98.9     | 0.13<br>0.07 | 99.5<br>99.5   |        |
| <i>Sub-solidus</i>                                       |           |         |  |                       |              |                    |              |                  |              |                |        |
| 18   | 1650      | 24      | $\alpha$ -C <sub>2</sub> S<br>C <sub>3</sub> S               | 66.8<br>75.0          | 0.09<br>0.15 | 0.0<br>0.0         | 0.00<br>0.00 | 33.2<br>25.0     | 0.09<br>0.08 | 97.9<br>100.0  |        |
| 19   | 1400      | 96      | C <sub>3</sub> S <sub>2</sub><br>CS                          | 60.0<br>50.0          | 0.20<br>0.14 | 0.0<br>0.0         | 0.00<br>0.00 | 40.0<br>50.0     | 0.20<br>0.13 | 100.4<br>100.6 |        |
| 20   | 1400      | 96      | $\alpha'$ -C <sub>2</sub> S<br>C <sub>3</sub> S <sub>2</sub> | 66.7<br>60.1          | 0.11<br>0.07 | 0.0<br>0.0         | 0.00<br>0.00 | 33.2<br>39.9     | 0.08<br>0.06 | 100.3<br>100.6 |        |
| 21   | 1400      | 96      | $\alpha'$ -C <sub>2</sub> S<br>C <sub>3</sub> S              | 66.7<br>75.0          | 0.07<br>0.15 | 0.0<br>0.0         | 0.00<br>0.00 | 33.3<br>25.0     | 0.07<br>0.14 | 100.4<br>100.7 |        |
| 22   | 1400      | 96      | C <sub>3</sub> S<br>lime                                     | 75.1<br>100.0         | 0.20<br>0.05 | 0.0<br>0.0         | 0.00<br>0.00 | 24.9<br>0.0      | 0.20<br>0.00 | 100.4<br>82.8  |        |
| 23   | 1300      | 96      | $\alpha'$ -C <sub>2</sub> S<br>C <sub>3</sub> S              | 67.1<br>75.1          | 0.02<br>0.36 | 0.0<br>0.0         | 0.00<br>0.00 | 32.9<br>24.9     | 0.04<br>0.35 | 100.9<br>100.9 |        |

Table V. continued

| No.  | Temp., °C | Time, h | Phase Assemblages | Composition (mol pct) |          |                    |          |                  |          | "Old Total"<br>(Wt Pct) |
|--|-----------|---------|-------------------|-----------------------|----------|--------------------|----------|------------------|----------|-------------------------|
|  |           |         |                   | CaO                   | St. Dev. | FeO <sub>1.5</sub> | St. Dev. | SiO <sub>2</sub> | St. Dev. |                         |
| "FeO <sub>1.5</sub> "-CaO-SiO <sub>2</sub> system in air       |           |         |                   |                       |          |                    |          |                  |          |                         |
| <i>Liquid in equilibrium with one solid (liquidus surface)</i> |           |         |                   |                       |          |                    |          |                  |          |                         |
| Spinel ppf.  |           |         |                   |                       |          |                    |          |                  |          |                         |
| 24   | 1500      | 4       | liq               | 10.4                  | 0.49     | 87.1               | 0.64     | 2.4              | 0.17     | 102.0                   |
|  |           |         | spinel            | 0.7                   | 0.04     | 99.3               | 0.04     | 0.0              | 0.00     | 103.5                   |
| 25   | 1500      | 4       | liq               | 7.5                   | 0.22     | 81.0               | 0.53     | 11.6             | 0.34     | 102.6                   |
|  |           |         | spinel            | 0.1                   | 0.00     | 99.9               | 0.03     | 0.0              | 0.02     | 103.3                   |
| 26   | 1400      | 16      | liq               | 20.3                  | 0.12     | 53.1               | 0.15     | 26.6             | 0.08     | 101.9                   |
|  |           |         | spinel            | 0.3                   | 0.05     | 99.7               | 0.08     | 0.0              | 0.02     | 104.1                   |
| Hematite ppf.  |           |         |                   |                       |          |                    |          |                  |          |                         |
| 27   | 1300      | 24      | liq               | 26.9                  | 0.11     | 31.1               | 0.12     | 42.0             | 0.11     | 100.8                   |
|  |           |         | hematite          | 0.0                   | 0.00     | 100.0              | 0.04     | 0.0              | 0.00     | 100.1                   |
| 28   | 1263      | 24      | liq               | 36.7                  | 0.13     | 43.4               | 0.12     | 19.9             | 0.05     | 100.6                   |
|  |           |         | hematite          | 0.0                   | 0.04     | 100.0              | 0.05     | 0.0              | 0.02     | 99.6                    |
| 29   | 1250      | 24      | liq               | 37.6                  | 0.10     | 42.3               | 0.11     | 20.1             | 0.11     | 101.1                   |
|  |           |         | hematite          | 0.0                   | 0.00     | 100.0              | 0.14     | 0.0              | 0.00     | 101.4                   |
| Lime ppf.  |           |         |                   |                       |          |                    |          |                  |          |                         |
| 30   | 1600      | 2       | liq               | 58.6                  | 0.14     | 38.5               | 0.13     | 2.9              | 0.03     | 99.2                    |
|  |           |         | lime              | 100.0                 | 0.06     | 0.0                | 0.00     | 0.0              | 0.00     | 83.3                    |
| 31   | 1435      | 16      | liq               | 56.4                  | 0.29     | 39.2               | 0.31     | 4.3              | 0.06     | 99.8                    |
|  |           |         | lime              | 100.0                 | 0.07     | 0.0                | 0.00     | 0.0              | 0.00     | 76.9                    |
| 32   | 1433      | 16      | liq               | 54.6                  | 0.19     | 44.8               | 0.19     | 0.5              | 0.02     | 99.1                    |
|  |           |         | lime              | 100.0                 | 0.30     | 0.0                | 0.00     | 0.0              | 0.00     | 67.6                    |
| 33   | 1425      | 16      | liq               | 56.3                  | 0.11     | 39.4               | 0.11     | 4.3              | 0.05     | 99.9                    |
|  |           |         | lime              | 100.0                 | 0.04     | 0.0                | 0.00     | 0.0              | 0.00     | 88.8                    |
| 34   | 1415      | 16      | liq               | 56.1                  | 0.28     | 39.6               | 0.27     | 4.2              | 0.03     | 99.9                    |
|  |           |         | lime              | 100.0                 | 0.04     | 0.0                | 0.00     | 0.0              | 0.00     | 99.9                    |
| Tridymite ppf.   |           |         |                   |                       |          |                    |          |                  |          |                         |
| 35   | 1400      | 24      | liq               | 27.2                  | 0.09     | 15.5               | 0.10     | 57.3             | 0.13     | 100.6                   |
|  |           |         | tridymite         | 0.1                   | 0.02     | 0.1                | 0.03     | 99.8             | 0.04     | 101.4                   |
| 36   | 1400      | 24      | liq               | 34.4                  | 0.07     | 4.9                | 0.06     | 60.7             | 0.07     | 100.6                   |
|  |           |         | tridymite         | 0.0                   | 0.00     | 0.1                | 0.02     | 99.9             | 0.04     | 100.0                   |
| 37   | 1400      | 24      | liq               | 22.9                  | 0.08     | 23.1               | 0.09     | 54.1             | 0.08     | 101.2                   |
|  |           |         | tridymite         | 0.1                   | 0.04     | 0.2                | 0.04     | 99.7             | 0.07     | 101.6                   |
| 38   | 1400      | 24      | liq               | 18.5                  | 0.08     | 32.3               | 0.10     | 49.1             | 0.07     | 101.8                   |
|  |           |         | tridymite         | 0.1                   | 0.01     | 0.2                | 0.04     | 99.7             | 0.05     | 101.9                   |
| 39   | 1300      | 24      | liq               | 24.7                  | 0.08     | 24.4               | 0.11     | 50.9             | 0.09     | 100.0                   |
|  |           |         | tridymite         | 0.1                   | 0.06     | 0.1                | 0.04     | 99.7             | 0.03     | 99.4                    |
| Cristobalite ppf.  |           |         |                   |                       |          |                    |          |                  |          |                         |
| 40   | 1695      | 1       | liq               | 22.4                  | 0.15     | 5.6                | 0.06     | 72.1             | 0.18     | 101.0                   |
|  |           |         | cristobalite      | n/a (*)               |          |                    |          |                  |          |                         |
| 41   | 1690      | 1       | liq               | 22.8                  | 0.09     | 5.4                | 0.09     | 71.7             | 0.12     | 100.1                   |
|  |           |         | cristobalite      | 0.2                   | 0.03     | 0.1                | 0.03     | 99.8             | 0.01     | 100.3                   |
| 42   | 1687      | 1       | liq               | 23.3                  | 0.17     | 5.7                | 0.08     | 71.0             | 0.21     | 100.5                   |
|  |           |         | cristobalite      | n/a (*)               |          |                    |          |                  |          |                         |
| 43   | 1685      | 1       | liq               | 10.9                  | 0.05     | 19.3               | 0.15     | 69.8             | 0.16     | 102.0                   |
|  |           |         | cristobalite      | 0.1                   | 0.02     | 0.3                | 0.03     | 99.6             | 0.05     | 100.1                   |
| 44   | 1680      | 1       | liq               | 23.6                  | 0.08     | 5.9                | 0.07     | 70.5             | 0.06     | 100.5                   |
|  |           |         | cristobalite      | 0.2                   | 0.03     | 0.1                | 0.01     | 99.7             | 0.04     | 101.6                   |
| 45   | 1650      | 1       | liq               | 19.6                  | 0.07     | 11.8               | 0.04     | 68.6             | 0.06     | 100.1                   |
|  |           |         | cristobalite      | 0.3                   | 0.16     | 0.2                | 0.03     | 99.5             | 0.16     | 99.5                    |
| 46   | 1650      | 1       | liq               | 10.3                  | 0.05     | 27.4               | 0.12     | 62.3             | 0.15     | 102.2                   |
|  |           |         | cristobalite      | 0.1                   | 0.07     | 0.4                | 0.06     | 99.5             | 0.07     | 100.7                   |
| 47   | 1600      | 2       | liq               | 28.8                  | 0.08     | 5.1                | 0.06     | 66.1             | 0.07     | 101.0                   |
|  |           |         | cristobalite      | 0.2                   | 0.03     | 0.1                | 0.02     | 99.7             | 0.04     | 101.5                   |
| 48   | 1600      | 2       | liq               | 12.0                  | 0.10     | 32.4               | 0.14     | 55.7             | 0.19     | 102.3                   |
|  |           |         | cristobalite      | 0.2                   | 0.03     | 0.4                | 0.03     | 99.4             | 0.06     | 100.5                   |
| 49   | 1600      | 2       | liq               | 4.5                   | 0.07     | 55.1               | 0.24     | 40.4             | 0.26     | 104.5                   |
|  |           |         | cristobalite      | 0.0                   | 0.00     | 0.3                | 0.10     | 99.6             | 0.12     | 100.6                   |



Table V. continued

| No.   | Temp., °C | Time, h | Phase Assemblages       | Composition (mol pct) |          |                    |          |                  |          | "Old Total"<br>(Wt Pct) |
|---|-----------|---------|-------------------------|-----------------------|----------|--------------------|----------|------------------|----------|-------------------------|
|   |           |         |                         | CaO                   | St. Dev. | FeO <sub>1.5</sub> | St. Dev. | SiO <sub>2</sub> | St. Dev. |                         |
| 50  | 1500      | 4       | liq                     | 31.7                  | 0.07     | 5.6                | 0.06     | 62.7             | 0.08     | 100.5                   |
|   |           |         | crystalite              | 0.2                   | 0.02     | 0.1                | 0.02     | 99.7             | 0.03     | 101.4                   |
| 51  | 1500      | 4       | liq                     | 13.7                  | 0.07     | 37.5               | 0.14     | 48.8             | 0.13     | 102.1                   |
|   |           |         | crystalite              | 0.1                   | 0.05     | 0.0                | 0.00     | 99.9             | 0.34     | 100.1                   |
| 52  | 1500      | 4       | liq                     | 5.2                   | 0.21     | 62.8               | 0.26     | 32.0             | 0.22     | 103.2                   |
|   |           |         | crystalite              | 0.2                   | 0.04     | 0.3                | 0.14     | 99.5             | 0.13     | 100.8                   |
| 53  | 1500      | 4       | liq                     | 21.2                  | 0.08     | 21.2               | 0.12     | 57.6             | 0.12     | 100.6                   |
|   |           |         | crystalite              | 0.1                   | 0.04     | 0.2                | 0.04     | 99.6             | 0.06     | 101.1                   |
| 54  | 1500      | 4       | liq                     | 16.9                  | 0.13     | 29.9               | 0.24     | 53.3             | 0.33     | 102.3                   |
|   |           |         | crystalite              | 0.2                   | 0.21     | 0.3                | 0.05     | 99.5             | 0.25     | 100.1                   |
| 55  | 1500      | 4       | liq                     | 25.0                  | 0.10     | 14.3               | 0.12     | 60.7             | 0.12     | 100.5                   |
|   |           |         | crystalite              | 0.3                   | 0.27     | 0.2                | 0.04     | 99.5             | 0.28     | 100.8                   |
| Pseudo-wollastonite (CS) ppf.                                 |           |         |                         |                       |          |                    |          |                  |          |                         |
| 56  | 1400      | 24      | liq                     | 38.3                  | 0.05     | 14.1               | 0.09     | 47.6             | 0.08     | 100.0                   |
|   |           |         | cs                      | 49.7                  | 0.06     | 0.0                | 0.00     | 50.3             | 0.05     | 100.5                   |
| 57  | 1300      | 24      | liq                     | 32.5                  | 0.07     | 21.2               | 0.05     | 46.3             | 0.08     | 100.0                   |
|   |           |         | cs                      | 49.9                  | 0.10     | 0.0                | 0.00     | 50.1             | 0.16     | 100.4                   |
| 58  | 1280      | 24      | liq                     | 37.9                  | 0.07     | 30.0               | 0.10     | 32.1             | 0.08     | 99.4                    |
|   |           |         | CS                      | 50.1                  | 0.06     | 0.0                | 0.03     | 49.9             | 0.07     | 99.6                    |
| Dicalcium Silicate (C <sub>2</sub> S) ppf.                    |           |         |                         |                       |          |                    |          |                  |          |                         |
| 59  | 1600      | 2       | liq                     | 49.3                  | 0.13     | 36.0               | 0.17     | 14.7             | 0.06     | 100.5                   |
|   |           |         | α-C <sub>2</sub> S      | 66.7                  | 0.11     | 0.5                | 0.07     | 32.8             | 0.10     | 100.7                   |
| 60  | 1600      | 2       | liq                     | 50.3                  | 0.08     | 22.6               | 0.11     | 27.0             | 0.10     | 99.8                    |
|   |           |         | α-C <sub>2</sub> S      | 66.2                  | 0.10     | 0.7                | 0.04     | 33.1             | 0.09     | 100.7                   |
| 61  | 1600      | 2       | liq                     | 57.7                  | 0.10     | 32.3               | 0.17     | 10.0             | 0.10     | 99.5                    |
|   |           |         | α-C <sub>2</sub> S      | 66.9                  | 0.11     | 1.6                | 0.06     | 31.5             | 0.10     | 100.3                   |
| 62  | 1500      | 4       | liq                     | 45.1                  | 0.10     | 43.8               | 0.16     | 11.2             | 0.08     | 101.1                   |
|   |           |         | α-C <sub>2</sub> S      | 66.4                  | 0.11     | 0.5                | 0.06     | 33.1             | 0.10     | 100.6                   |
| 63  | 1500      | 4       | liq                     | 46.8                  | 0.07     | 29.0               | 0.08     | 24.3             | 0.05     | 100.6                   |
|   |           |         | α-C <sub>2</sub> S      | 66.0                  | 0.13     | 0.8                | 0.08     | 33.2             | 0.08     | 100.5                   |
| 64  | 1500      | 4       | liq                     | 52.1                  | 0.13     | 40.3               | 0.14     | 7.6              | 0.04     | 99.4                    |
|   |           |         | α-C <sub>2</sub> S      | 66.8                  | 0.18     | 1.1                | 0.10     | 32.1             | 0.10     | 100.0                   |
| 65  | 1440      | 16      | liq                     | 43.7                  | 0.08     | 47.6               | 0.14     | 8.6              | 0.12     | 98.9                    |
|   |           |         | α-C <sub>2</sub> S(**)  | 66.5                  | 0.23     | 0.5                | 0.07     | 33.1             | 0.24     | 100.6                   |
| 66  | 1430      | 16      | liq                     | 43.4                  | 0.57     | 48.2               | 0.62     | 8.5              | 0.09     | 101.3                   |
|   |           |         | α'-C <sub>2</sub> S(**) | n/a (*)               |          |                    |          |                  |          |                         |
| 67  | 1400      | 16      | liq                     | 51.4                  | 0.08     | 10.7               | 0.13     | 37.9             | 0.10     | 100.0                   |
|   |           |         | α'-C <sub>2</sub> S     | 65.5                  | 0.18     | 1.1                | 0.06     | 33.3             | 0.13     | 100.9                   |
| 68  | 1400      | 16      | liq                     | 45.0                  | 0.20     | 29.6               | 0.24     | 25.4             | 0.13     | 99.8                    |
|   |           |         | α'-C <sub>2</sub> S     | 66.4                  | 0.25     | 0.5                | 0.00     | 33.1             | 0.25     | 99.8                    |
| 69  | 1400      | 16      | liq                     | 52.3                  | 0.14     | 9.1                | 0.08     | 38.7             | 0.14     | 100.0                   |
|   |           |         | α'-C <sub>2</sub> S     | 65.8                  | 0.20     | 0.9                | 0.05     | 33.3             | 0.18     | 99.9                    |
| 70  | 1400      | 16      | liq                     | 48.3                  | 0.32     | 46.0               | 0.32     | 5.7              | 0.05     | 100.4                   |
|   |           |         | α'-C <sub>2</sub> S     | 66.6                  | 0.16     | 0.4                | 0.18     | 33.0             | 0.16     | 98.9                    |
| 71  | 1300      | 24      | liq                     | 40.2                  | 0.08     | 37.9               | 0.09     | 21.9             | 0.09     | 100.4                   |
|   |           |         | α'-C <sub>2</sub> S     | 66.7                  | 0.13     | 0.0                | 0.00     | 33.3             | 0.14     | 101.0                   |
| 72  | 1300      | 24      | liq                     | 43.8                  | 0.12     | 27.2               | 0.10     | 28.9             | 0.08     | 100.9                   |
|   |           |         | α'-C <sub>2</sub> S     | 66.6                  | 0.09     | 0.0                | 0.00     | 33.4             | 0.07     | 101.4                   |
| 73  | 1300      | 24      | liq                     | 41.0                  | 0.07     | 35.7               | 0.17     | 23.3             | 0.14     | 100.1                   |
|   |           |         | α'-C <sub>2</sub> S     | 66.7                  | 0.09     | 0.0                | 0.00     | 33.3             | 0.01     | 100.4                   |
| <i>Liquid in equilibrium with two solids (boundary lines)</i> |           |         |                         |                       |          |                    |          |                  |          |                         |
| Hematite – Dicalcium Silicate (C <sub>2</sub> S) boundary     |           |         |                         |                       |          |                    |          |                  |          |                         |
| 74  | 1240      | 24      | liq                     | 39.8                  | 0.17     | 36.3               | 0.28     | 23.9             | 0.29     | 100.5                   |
|   |           |         | hematite                | 0.1                   | 0.09     | 99.8               | 0.11     | 0.1              | 0.02     | 100.5                   |
|   |           |         | α'-C <sub>2</sub> S     | 66.7                  | 0.21     | 0.6                | 0.14     | 32.7             | 0.15     | 100.2                   |
| 75  | 1235      | 24      | liq                     | 41.2                  | 0.19     | 32.7               | 0.18     | 26.1             | 0.17     | 100.3                   |
|   |           |         | hematite                | 0.1                   | 0.10     | 99.9               | 0.08     | 0.0              | 0.00     | 100.1                   |
|   |           |         | α'-C <sub>2</sub> S     | 67.1                  | 0.50     | 0.2                | 0.38     | 32.7             | 0.23     | 101.2                   |

Table V. continued

| No.   | Temp., °C | Time, h | Phase Assemblages             | Composition (mol pct) |          |                    |          |                  |          | "Old Total" (Wt Pct) |
|---|-----------|---------|-------------------------------|-----------------------|----------|--------------------|----------|------------------|----------|----------------------|
|   |           |         |                               | CaO                   | St. Dev. | FeO <sub>1.5</sub> | St. Dev. | SiO <sub>2</sub> | St. Dev. |                      |
| Hematite – Tridymite boundary   |           |         |                               |                       |          |                    |          |                  |          |                      |
| 76  | 1385      | 24      | liq                           | 12.7                  | 0.31     | 48.1               | 0.27     | 39.2             | 0.27     | 100.2                |
|   |           |         | hematite                      | 0.0                   | 0.00     | 100.0              | 0.03     | 0.0              | 0.00     | 99.4                 |
|   |           |         | tridymite                     | 0.1                   | 0.01     | 0.2                | 0.10     | 99.7             | 0.12     | 100.8                |
| 77  | 1350      | 24      | liq                           | 16.9                  | 0.08     | 38.6               | 0.13     | 44.6             | 0.90     | 101.2                |
|   |           |         | hematite                      | 0.0                   | 0.00     | 100.0              | 0.03     | 0.0              | 0.00     | 100.1                |
|   |           |         | tridymite                     | 0.0                   | 0.02     | 0.3                | 0.17     | 99.7             | 0.17     | 102.4                |
| 78  | 1300      | 24      | liq                           | 21.8                  | 0.08     | 29.9               | 0.09     | 48.3             | 0.10     | 101.2                |
|   |           |         | hematite                      | 0.0                   | 0.00     | 99.8               | 0.04     | 0.2              | 0.04     | 100.1                |
|   |           |         | tridymite                     | 0.0                   | 0.00     | 0.2                | 0.06     | 99.8             | 0.08     | 101.1                |
| Spinel – Tridymite boundary   |           |         |                               |                       |          |                    |          |                  |          |                      |
| 79  | 1390      | 24      | liq                           | 11.9                  | 0.31     | 50.5               | 0.26     | 37.6             | 0.16     | 102.2                |
|   |           |         | Spinel                        | 0.0                   | 0.00     | 100.0              | 0.06     | 0.0              | 0.00     | 103.1                |
|   |           |         | tridymite                     | 0.1                   | 0.04     | 0.2                | 0.12     | 99.7             | 0.13     | 102.6                |
| Hematite – Pseudo-wollastonite (CS) boundary  |           |         |                               |                       |          |                    |          |                  |          |                      |
| 80  | 1280      | 24      | liq                           | 33.0                  | 0.12     | 29.5               | 0.12     | 37.5             | 0.09     | 99.6                 |
|   |           |         | hematite                      | 0.3                   | 0.16     | 99.7               | 0.17     | 0.0              | 0.00     | 100.2                |
|   |           |         | CS                            | 50.0                  | 0.06     | 0.1                | 0.03     | 49.9             | 0.06     | 99.6                 |
| 81  | 1260      | 24      | liq                           | 38.6                  | 0.08     | 30.8               | 0.11     | 30.6             | 0.08     | 100.4                |
|   |           |         | hematite                      | 0.1                   | 0.02     | 99.9               | 0.06     | 0.0              | 0.00     | 100.2                |
|   |           |         | CS                            | 50.3                  | 0.09     | 0.0                | 0.00     | 49.7             | 0.09     | 100.7                |
| 82  | 1250      | 24      | liq                           | 31.0                  | 0.09     | 26.7               | 0.17     | 42.2             | 0.11     | 100.0                |
|   |           |         | hematite                      | 0.2                   | 0.06     | 99.8               | 0.07     | 0.0              | 0.00     | 100.1                |
|   |           |         | CS                            | 50.0                  | 0.08     | 0.1                | 0.06     | 49.9             | 0.08     | 101.3                |
| 83  | 1240      | 24      | liq                           | 30.4                  | 0.09     | 26.0               | 0.17     | 43.6             | 0.11     | 99.4                 |
|   |           |         | hematite                      | 0.3                   | 0.15     | 99.7               | 0.08     | 0.0              | 0.00     | 99.5                 |
|   |           |         | CS                            | 49.9                  | 0.04     | 0.1                | 0.05     | 50.0             | 0.04     | 100.0                |
| 84  | 1205      | 24      | liq                           | 27.8                  | 0.07     | 22.9               | 0.06     | 49.2             | 0.12     | 100.2                |
|   |           |         | hematite                      | 0.1                   | 0.08     | 99.8               | 0.11     | 0.1              | 0.03     | 100.3                |
|   |           |         | CS                            | 49.8                  | 0.18     | 0.2                | 0.15     | 50.0             | 0.09     | 100.9                |
| Pseudo-wollastonite (CS) – Tridymite boundary   |           |         |                               |                       |          |                    |          |                  |          |                      |
| 85  | 1300      | 24      | liq                           | 30.5                  | 0.09     | 13.5               | 0.06     | 56.1             | 0.09     | 99.7                 |
|   |           |         | tridymite                     | 0.2                   | 0.05     | 0.0                | 0.00     | 99.8             | 0.08     | 100.4                |
|   |           |         | CS                            | 50.0                  | 0.16     | 0.0                | 0.00     | 50.0             | 0.17     | 100.0                |
| Rankinite (C <sub>3</sub> S <sub>2</sub> ) – Pseudo-wollastonite (CS) boundary              |           |         |                               |                       |          |                    |          |                  |          |                      |
| 86  | 1400      | 16      | liq                           | 52.0                  | 0.12     | 7.5                | 0.15     | 40.5             | 0.08     | 99.8                 |
|   |           |         | C <sub>3</sub> S <sub>2</sub> | 59.9                  | 0.08     | 0.0                | 0.04     | 40.1             | 0.08     | 100.0                |
|   |           |         | CS                            | 49.8                  | 0.11     | 0.1                | 0.02     | 50.1             | 0.11     | 100.2                |
| 87  | 1300      | 24      | liq                           | 46.3                  | 0.07     | 19.1               | 0.11     | 34.6             | 0.09     | 99.9                 |
|   |           |         | C <sub>3</sub> S <sub>2</sub> | 60.0                  | 0.04     | 0.0                | 0.00     | 39.9             | 0.04     | 100.5                |
|   |           |         | CS                            | 50.1                  | 0.10     | 0.0                | 0.00     | 49.9             | 0.12     | 100.6                |
| 88  | 1250      | 24      | liq                           | 42.7                  | 0.09     | 26.4               | 0.08     | 30.9             | 0.07     | 100.2                |
|   |           |         | C <sub>3</sub> S <sub>2</sub> | 60.0                  | 0.10     | 0.0                | 0.04     | 40.0             | 0.11     | 101.3                |
|   |           |         | CS                            | 49.9                  | 0.14     | 0.1                | 0.08     | 50.0             | 0.11     | 101.0                |
| 89  | 1235      | 24      | liq                           | 41.3                  | 0.09     | 29.1               | 0.10     | 29.5             | 0.08     | 100.0                |
|   |           |         | C <sub>3</sub> S <sub>2</sub> | 59.9                  | 0.07     | 0.0                | 0.06     | 40.1             | 0.09     | 100.2                |
|   |           |         | CS                            | 49.9                  | 0.04     | 0.1                | 0.08     | 50.0             | 0.09     | 100.5                |
| 90  | 1230      | 24      | liq                           | 41.3                  | 0.09     | 29.4               | 0.09     | 29.3             | 0.04     | 100.1                |
|   |           |         | C <sub>3</sub> S <sub>2</sub> | 60.1                  | 0.10     | 0.0                | 0.03     | 39.9             | 0.03     | 101.0                |
|   |           |         | CS                            | 49.9                  | 0.08     | 0.0                | 0.02     | 50.1             | 0.08     | 101.0                |
| 91  | 1225      | 24      | liq                           | 41.0                  | 0.10     | 29.7               | 0.14     | 29.3             | 0.09     | 99.4                 |
|   |           |         | C <sub>3</sub> S <sub>2</sub> | 59.8                  | 0.10     | 0.0                | 0.00     | 40.2             | 0.07     | 101.2                |
|   |           |         | CS                            | 49.7                  | 0.03     | 0.0                | 0.00     | 50.3             | 0.07     | 101.3                |
| Rankinite (C <sub>3</sub> S <sub>2</sub> ) – Dicalcium Silicate (C <sub>2</sub> S) boundary |           |         |                               |                       |          |                    |          |                  |          |                      |
| 92  | 1410      | 16      | liq                           | 53.5                  | 0.10     | 6.1                | 0.09     | 40.4             | 0.13     | 99.8                 |
|   |           |         | C <sub>3</sub> S <sub>2</sub> | 60.0                  | 0.12     | 0.0                | 0.00     | 40.0             | 0.14     | 100.3                |

Table V. continued

| No.  | Temp., °C | Time, h | Phase Assemblages             | Composition (mol pct) |          |                    |          |                  |          | "Old Total" (Wt Pct) |
|--|-----------|---------|-------------------------------|-----------------------|----------|--------------------|----------|------------------|----------|----------------------|
|  |           |         |                               | CaO                   | St. Dev. | FeO <sub>1.5</sub> | St. Dev. | SiO <sub>2</sub> | St. Dev. |                      |
| 93   | 1350      | 24      | $\alpha'$ -C <sub>2</sub> S   | 65.8                  | 0.14     | 0.8                | 0.05     | 33.3             | 0.13     | 100.4                |
|  |           |         | liq                           | 49.8                  | 0.13     | 13.7               | 0.11     | 36.5             | 0.09     | 100.0                |
|  |           |         | C <sub>3</sub> S <sub>2</sub> | 60.1                  | 0.06     | 0.0                | 0.01     | 39.9             | 0.08     | 100.7                |
| 94   | 1300      | 24      | $\alpha'$ -C <sub>2</sub> S   | 66.7                  | 0.32     | 0.1                | 0.07     | 33.2             | 0.34     | 100.4                |
|  |           |         | liq                           | 46.1                  | 0.09     | 21.6               | 0.14     | 32.3             | 0.09     | 99.9                 |
|  |           |         | C <sub>3</sub> S <sub>2</sub> | 60.1                  | 0.07     | 0.0                | 0.03     | 39.9             | 0.07     | 101.0                |
| 95   | 1275      | 24      | $\alpha'$ -C <sub>2</sub> S   | 66.8                  | 0.19     | 0.1                | 0.07     | 33.2             | 0.16     | 100.7                |
|  |           |         | liq                           | 44.0                  | 0.12     | 26.4               | 0.20     | 29.6             | 0.12     | 99.4                 |
|  |           |         | C <sub>3</sub> S <sub>2</sub> | 60.1                  | 0.06     | 0.0                | 0.00     | 39.9             | 0.03     | 100.2                |
| 96   | 1260      | 24      | $\alpha'$ -C <sub>2</sub> S   | 66.8                  | 0.14     | 0.1                | 0.06     | 33.1             | 0.11     | 98.8                 |
|  |           |         | liq                           | 42.9                  | 0.09     | 28.6               | 0.08     | 28.5             | 0.06     | 99.0                 |
|  |           |         | C <sub>3</sub> S <sub>2</sub> | 60.1                  | 0.11     | 0.0                | 0.04     | 39.9             | 0.10     | 99.7                 |
| 97   | 1235      | 24      | $\alpha'$ -C <sub>2</sub> S   | 66.8                  | 0.15     | 0.1                | 0.07     | 33.1             | 0.14     | 99.3                 |
|  |           |         | liq                           | 41.0                  | 0.12     | 33.1               | 0.14     | 25.9             | 0.16     | 99.6                 |
|  |           |         | C <sub>3</sub> S <sub>2</sub> | 60.1                  | 0.17     | 0.0                | 0.05     | 39.9             | 0.16     | 100.3                |
| Dicalcium Ferrite (C <sub>2</sub> F) – Dicalcium Silicate (C <sub>2</sub> S) boundary<br>98    | 1410      | 16      | liq                           | 55.5                  | 0.10     | 38.9               | 0.10     | 5.6              | 0.03     | 99.9                 |
|  |           |         | C <sub>2</sub> F              | 50.3                  | 0.13     | 49.5               | 0.14     | 0.1              | 0.03     | 100.1                |
|  |           |         | $\alpha'$ -C <sub>2</sub> S   | 66.6                  | 0.11     | 2.4                | 0.10     | 31.0             | 0.13     | 99.8                 |
| 99   | 1410      | 16      | liq                           | 50.6                  | 0.15     | 43.8               | 0.13     | 5.6              | 0.06     | 100.2                |
|  |           |         | C <sub>2</sub> F              | 50.6                  | 0.09     | 48.7               | 0.17     | 0.7              | 0.12     | 100.1                |
|  |           |         | $\alpha'$ -C <sub>2</sub> S   | 66.3                  | 0.43     | 0.6                | 0.21     | 33.1             | 0.38     | 99.1                 |
| 100  | 1390      | 16      | liq                           | 47.2                  | 0.24     | 47.6               | 0.26     | 5.2              | 0.06     | 99.4                 |
|  |           |         | C <sub>2</sub> F              | 50.6                  | 0.14     | 48.8               | 0.20     | 0.6              | 0.07     | 99.5                 |
|  |           |         | $\alpha'$ -C <sub>2</sub> S   | 66.6                  | 0.03     | 0.3                | 0.05     | 33.1             | 0.05     | 99.4                 |
| 101  | 1340      | 24      | liq                           | 42.7                  | 0.47     | 52.3               | 0.56     | 4.9              | 0.15     | 99.7                 |
|  |           |         | C <sub>2</sub> F              | 50.4                  | 0.06     | 48.8               | 0.14     | 0.8              | 0.12     | 99.0                 |
|  |           |         | $\alpha'$ -C <sub>2</sub> S   | 66.5                  | 0.45     | 0.4                | 0.47     | 33.1             | 0.14     | 99.2                 |
| Dicalcium Ferrite (C <sub>2</sub> F) – Lime boundary<br>102                                    | 1410      | 16      | liq                           | 56.2                  | 0.25     | 39.1               | 0.21     | 4.7              | 0.23     | 100.4                |
|  |           |         | lime                          | 99.9                  | 0.21     | 0.1                | 0.20     | 0.0              | 0.00     | 101.1                |
|  |           |         | C <sub>2</sub> F              | 50.5                  | 0.14     | 49.1               | 0.21     | 0.5              | 0.14     | 100.5                |
| Lime – Tricalcium Silicate (C <sub>3</sub> S) boundary<br>103                                  | 1685      | 1       | liq                           | 62.9                  | 0.12     | 24.9               | 0.19     | 12.2             | 0.17     | 99.8                 |
|  |           |         | lime                          | 99.8                  | 0.05     | 0.2                | 0.05     | 0.0              | 0.00     | 98.7                 |
|  |           |         | C <sub>3</sub> S              | 74.5                  | 0.17     | 1.1                | 0.24     | 24.4             | 0.22     | 100.3                |
| 104  | 1650      | 1       | liq                           | 62.3                  | 0.18     | 26.9               | 0.20     | 10.8             | 0.05     | 101.1                |
|  |           |         | lime                          | 99.8                  | 0.10     | 0.2                | 0.08     | 0.0              | 0.00     | 102.2                |
|  |           |         | C <sub>3</sub> S              | 74.8                  | 0.07     | 1.0                | 0.18     | 24.2             | 0.16     | 102.1                |
| 105  | 1600      | 1       | liq                           | 61.1                  | 0.27     | 29.3               | 0.34     | 9.6              | 0.13     | 99.5                 |
|  |           |         | lime                          | 99.9                  | 0.07     | 0.1                | 0.07     | 0.0              | 0.00     | 100.3                |
|  |           |         | C <sub>3</sub> S              | 74.8                  | 0.15     | 1.1                | 0.11     | 24.1             | 0.18     | 101.0                |
| 106  | 1550      | 2       | liq                           | 59.9                  | 0.10     | 32.0               | 0.07     | 8.1              | 0.04     | 99.9                 |
|  |           |         | lime                          | 99.8                  | 0.08     | 0.2                | 0.07     | 0.0              | 0.00     | 94.5                 |
|  |           |         | C <sub>3</sub> S              | 74.7                  | 0.18     | 1.1                | 0.27     | 24.2             | 0.19     | 101.0                |
| 107  | 1500      | 4       | liq                           | 58.1                  | 0.10     | 34.9               | 0.09     | 7.0              | 0.03     | 100.2                |
|  |           |         | lime                          | 100.0                 | 0.07     | 0.0                | 0.00     | 0.0              | 0.00     | 78.8                 |
|  |           |         | C <sub>3</sub> S              | 74.4                  | 0.42     | 1.1                | 0.24     | 24.4             | 0.44     | 100.7                |
| 108  | 1440      | 4       | liq                           | 56.9                  | 0.09     | 37.6               | 0.10     | 5.5              | 0.02     | 100.2                |
|  |           |         | lime                          | 100.0                 | 0.05     | 0.0                | 0.00     | 0.0              | 0.00     | 99.9                 |
|  |           |         | C <sub>3</sub> S              | 74.2                  | 0.25     | 1.1                | 0.27     | 24.7             | 0.32     | 100.0                |
| Dicalcium Silicate (C <sub>2</sub> S) – Tricalcium Silicate (C <sub>3</sub> S) boundary<br>109 | 1685      | 1       | liq                           | 62.6                  | 0.23     | 23.8               | 0.34     | 13.6             | 0.20     | 99.9                 |
|  |           |         | $\alpha'$ -C <sub>2</sub> S   | 66.8                  | 0.20     | 2.1                | 0.13     | 31.1             | 0.21     | 99.1                 |
|  |           |         | C <sub>3</sub> S              | 74.7                  | 0.13     | 0.9                | 0.18     | 24.4             | 0.15     | 100.4                |

Table V. continued

| No.   | Temp., °C | Time, h | Phase Assemblages               | Composition (mol pct) |          |                    |          |                  |          | "Old Total" (Wt Pct) |
|---|-----------|---------|---------------------------------|-----------------------|----------|--------------------|----------|------------------|----------|----------------------|
|   |           |         |                                 | CaO                   | St. Dev. | FeO <sub>1.5</sub> | St. Dev. | SiO <sub>2</sub> | St. Dev. |                      |
| 110   | 1650      | 1       | liq                             | 62.1                  | 0.12     | 25.4               | 0.12     | 12.5             | 0.05     | 100.8                |
|   |           |         | $\alpha$ -C <sub>2</sub> S      | 66.6                  | 0.09     | 2.1                | 0.11     | 31.0             | 0.18     | 101.5                |
|   |           |         | C <sub>3</sub> S                | 74.6                  | 0.10     | 1.1                | 0.12     | 24.3             | 0.10     | 101.8                |
| 111   | 1600      | 1       | liq                             | 60.5                  | 0.13     | 28.7               | 0.14     | 10.8             | 0.04     | 100.4                |
|   |           |         | $\alpha$ -C <sub>2</sub> S      | 66.9                  | 0.10     | 2.3                | 0.10     | 30.8             | 0.10     | 101.3                |
|   |           |         | C <sub>3</sub> S                | 74.6                  | 0.10     | 1.0                | 0.18     | 24.4             | 0.14     | 101.5                |
| 112   | 1550      | 2       | liq                             | 59.6                  | 0.14     | 31.3               | 0.20     | 9.1              | 0.08     | 100.4                |
|   |           |         | $\alpha$ -C <sub>2</sub> S      | 66.8                  | 0.10     | 2.3                | 0.08     | 30.9             | 0.11     | 102.0                |
|   |           |         | C <sub>3</sub> S                | 74.7                  | 0.13     | 1.0                | 0.22     | 24.3             | 0.19     | 102.0                |
| 113   | 1500      | 4       | liq                             | 57.8                  | 0.05     | 34.5               | 0.08     | 7.7              | 0.05     | 99.6                 |
|   |           |         | $\alpha$ -C <sub>2</sub> S      | 66.8                  | 0.13     | 2.6                | 0.11     | 30.6             | 0.20     | 99.3                 |
|   |           |         | C <sub>3</sub> S                | 74.4                  | 0.10     | 1.1                | 0.10     | 24.4             | 0.12     | 100.5                |
| 114   | 1450      | 4       | liq                             | 56.7                  | 0.09     | 37.0               | 0.14     | 6.3              | 0.06     | 100.0                |
|   |           |         | $\alpha'$ -C <sub>2</sub> S(**) | 66.6                  | 0.16     | 2.8                | 0.05     | 30.6             | 0.15     | 100.4                |
|   |           |         | C <sub>3</sub> S                | 74.1                  | 0.30     | 1.3                | 0.37     | 24.7             | 0.21     | 100.5                |
| 115   | 1440      | 4       | liq                             | 56.4                  | 0.16     | 37.4               | 0.15     | 6.2              | 0.05     | 100.3                |
|   |           |         | $\alpha'$ -C <sub>2</sub> S(**) | 66.5                  | 0.12     | 2.5                | 0.05     | 31.0             | 0.08     | 99.9                 |
|   |           |         | C <sub>3</sub> S                | 73.9                  | 0.27     | 1.5                | 0.09     | 24.7             | 0.19     | 100.3                |
| 116   | 1430      | 4       | liq                             | 56.3                  | 0.18     | 37.7               | 0.14     | 6.0              | 0.06     | 98.5                 |
|   |           |         | $\alpha'$ -C <sub>2</sub> S(**) | 66.9                  | 0.05     | 2.5                | 0.04     | 30.6             | 0.02     | 99.9                 |
|   |           |         | C <sub>3</sub> S                | 74.3                  | 0.23     | 1.1                | 0.25     | 24.7             | 0.22     | 99.8                 |
| <i>Two immiscible liquids</i>                                   |           |         |                                 |                       |          |                    |          |                  |          |                      |
| 117   | 1686      | 1       | liq 1                           | 16.5                  | 0.27     | 11.8               | 0.20     | 71.7             | 0.47     | 100.5                |
|   |           |         | liq 2                           | 2.8                   | 0.12     | 2.7                | 0.11     | 94.5             | 0.22     | 100.9                |
|   |           |         | crystalite                      | 0.1                   | 0.06     | 0.3                | 0.05     | 99.6             | 0.10     | 100.8                |
| 118   | 1685      | 1       | liq 1                           | 10.2                  | 0.12     | 17.8               | 0.12     | 72.0             | 0.23     | 98.5                 |
|   |           |         | liq 2                           | 2.4                   | 0.12     | 4.6                | 0.20     | 93.0             | 0.31     | 97.2                 |
|   |           |         | crystalite                      | 0.1                   | 0.06     | 0.3                | 0.05     | 99.6             | 0.10     | 100.8                |
| 119   | 1683      | 1       | liq 1                           | 8.3                   | 0.03     | 26.2               | 0.15     | 65.5             | 0.13     | 102.9                |
|   |           |         | liq 2                           | 1.2                   | 0.05     | 4.0                | 0.13     | 94.8             | 0.18     | 100.6                |
|   |           |         | crystalite                      | 0.1                   | 0.06     | 0.3                | 0.05     | 99.6             | 0.10     | 100.8                |
| 120   | 1683      | 1       | liq 1                           | 8.5                   | 0.05     | 26.0               | 0.14     | 65.5             | 0.18     | 102.6                |
|   |           |         | liq 2                           | 1.3                   | 0.07     | 4.1                | 0.19     | 94.6             | 0.25     | 100.4                |
|   |           |         | crystalite                      | 0.1                   | 0.06     | 0.3                | 0.05     | 99.6             | 0.10     | 100.8                |
| 121   | 1682      | 1       | liq 1                           | 6.5                   | 0.06     | 36.1               | 0.14     | 57.4             | 0.18     | 103.6                |
|   |           |         | liq 2                           | 0.8                   | 0.09     | 4.1                | 0.29     | 95.1             | 0.39     | 100.7                |
|   |           |         | crystalite                      | 0.1                   | 0.06     | 0.3                | 0.05     | 99.6             | 0.10     | 100.8                |
| 122   | 1681      | 1       | liq 1                           | 4.0                   | 0.18     | 46.1               | 0.96     | 49.9             | 0.99     | 103.4                |
|   |           |         | liq 2                           | 0.3                   | 0.03     | 3.2                | 0.15     | 96.4             | 0.18     | 99.4                 |
|   |           |         | crystalite                      | 0.1                   | 0.06     | 0.4                | 0.27     | 99.5             | 0.29     | 99.1                 |
| <i>Hematite + Pseudo-wollastonite (CS) + Tridymite eutectic</i> |           |         |                                 |                       |          |                    |          |                  |          |                      |
| 123 (***)   | 1199      | 24      | liq                             | 27.4                  | 0.10     | 22.1               | 0.10     | 50.5             | 0.11     | 100.0                |
|   |           |         | hematite                        | 0.0                   | 0.00     | 99.8               | 0.03     | 0.1              | 0.01     | 100.6                |
|   |           |         | CS                              | 49.8                  | 0.18     | 0.1                | 0.12     | 50.0             | 0.13     | 101.2                |
|   |           |         | tridymite                       | 0.1                   | 0.08     | 0.2                | 0.08     | 99.7             | 0.12     | 101.1                |
| 124 (***)   | 1199      | 24      | liq                             | 27.4                  | 0.09     | 22.1               | 0.09     | 50.5             | 0.11     | 99.9                 |
|   |           |         | hematite                        | 0.0                   | 0.00     | 99.9               | 0.15     | 0.1              | 0.02     | 100.1                |
|   |           |         | CS                              | 49.7                  | 0.12     | 0.1                | 0.09     | 50.2             | 0.12     | 100.3                |
|   |           |         | tridymite                       | 0.1                   | 0.02     | 0.2                | 0.06     | 99.7             | 0.04     | 100.3                |
| <i>Sub-solidus</i>  |           |         |                                 |                       |          |                    |          |                  |          |                      |
| 125   | 1400      | 24      | lime                            | 100.0                 | 0.26     | 0.0                | 0.00     | 0.0              | 0.00     | 88.3                 |
|   |           |         | C <sub>3</sub> S                | 74.3                  | 0.29     | 1.2                | 0.19     | 24.4             | 0.20     | 100.9                |
|   |           |         | C <sub>2</sub> F                | 50.4                  | 0.11     | 49.1               | 0.17     | 0.5              | 0.13     | 100.2                |
| 126   | 1400      | 24      | $\alpha'$ -C <sub>2</sub> S     | 66.9                  | 0.30     | 2.2                | 0.20     | 30.9             | 0.14     | 100.2                |
|   |           |         | C <sub>3</sub> S                | 74.7                  | 0.15     | 1.1                | 0.17     | 24.2             | 0.17     | 100.4                |
|   |           |         | C <sub>2</sub> F                | 50.4                  | 0.16     | 49.6               | 0.16     | 0.0              | 0.00     | 99.8                 |
| 127   | 1230      | 72      | C <sub>3</sub> S <sub>2</sub>   | 59.9                  | 0.06     | 0.0                | 0.14     | 40.1             | 0.09     | 101.2                |
|   |           |         | $\alpha'$ -C <sub>2</sub> S     | 66.6                  | 0.10     | 0.0                | 0.00     | 33.4             | 0.08     | 101.2                |
|   |           |         | hematite                        | 0.0                   | 0.00     | 100.0              | 0.02     | 0.0              | 0.00     | 99.8                 |

Table V. continued

| No. | Temp., °C | Time, h | Phase Assemblages             | Composition (mol pct) |          |                    |          |                  |          | “Old Total” (Wt Pct) |
|-----|-----------|---------|-------------------------------|-----------------------|----------|--------------------|----------|------------------|----------|----------------------|
|     |           |         |                               | CaO                   | St. Dev. | FeO <sub>1.5</sub> | St. Dev. | SiO <sub>2</sub> | St. Dev. |                      |
| 128 | 1220      | 72      | C <sub>3</sub> S <sub>2</sub> | 60.0                  | 0.03     | 0.1                | 0.02     | 39.8             | 0.02     | 100.7                |
|     |           |         | CS                            | 50.2                  | 0.21     | 0.0                | 0.00     | 49.8             | 0.16     | 100.6                |
|     |           |         | hematite                      | 0.0                   | 0.00     | 100.0              | 0.04     | 0.0              | 0.00     | 100.0                |

(\*) no accurate measurement due to small phase size; (\*\*) Characterization of different polymorphs of C<sub>2</sub>S ( $\alpha$ - and  $\alpha'$ -) is out of scope in the present study and their transition temperature is accepted at 1439 °C from a recent thermodynamic optimization by Shevchenko *et al.*<sup>[54]</sup>; (\*\*\*) Metastable phase due to (i) insufficient reaction time; (ii) minor impurity (< 0.1 mol pct); or (iii) local temperature fluctuation due to furnace control.

wollastonite (CaSiO<sub>3</sub>) and rankinite (Ca<sub>3</sub>Si<sub>2</sub>O<sub>7</sub>) is applied for other calcium silicates (Ca<sub>x</sub>Si<sub>y</sub>O<sub>z</sub>) such as dicalcium silicate (Ca<sub>2</sub>SiO<sub>4</sub>) and tricalcium silicate (Ca<sub>3</sub>SiO<sub>5</sub>). No significant secondary fluorescence was detected for: (i) SiO<sub>2</sub> on calcium ferrites, (ii) SiO<sub>2</sub> on hematite and (iii) CaO in spinel, therefore the measured non-stoichiometric compositions (if any) of these solids will be considered as true solubility unless further research proves otherwise. The following corrections for the secondary X-ray fluorescence have therefore been developed and applied in the present study to the compositions of all calcium silicates, lime, tridymite, cristobalite phases surrounded by liquid slag measured by EPMA.

$$\begin{aligned} \text{wt pct}(\text{Fe}_2\text{O}_3 \text{ in Ca}_x\text{Si}_y\text{O}_z)^{\text{corr}} &= \text{wt pct}(\text{Fe}_2\text{O}_3 \text{ in Ca}_x\text{Si}_y\text{O}_z)^{\text{initial}} \\ &\quad - 0.007 \text{ wt pct}(\text{Fe}_2\text{O}_3 \text{ in slag})^{\text{initial}} \\ \text{wt pct}(\text{Fe}_2\text{O}_3 \text{ in SiO}_2)^{\text{corr}} &= \text{wt pct}(\text{Fe}_2\text{O}_3 \text{ in SiO}_2)^{\text{initial}} \\ &\quad - 0.011 \text{ wt pct}(\text{Fe}_2\text{O}_3 \text{ in slag})^{\text{initial}} \\ \text{wt pct}(\text{Fe}_2\text{O}_3 \text{ in CaO})^{\text{corr}} &= \text{wt pct}(\text{Fe}_2\text{O}_3 \text{ in CaO})^{\text{initial}} \\ &\quad - 0.013 \text{ wt pct}(\text{Fe}_2\text{O}_3 \text{ in slag})^{\text{initial}} \end{aligned}$$

A 4-points test approach<sup>[40]</sup> was applied to confirm the equilibrium achievement, which includes: (i) Test of the effect of equilibration time; (ii) Analysis of the homogeneity of phases; (iii) Evaluation of the effect of direction of approach toward the equilibrium point; and (iv) Systematic analysis of reactions specific to the system. In the present study,

1. Test of the equilibration time was carried out in a previous study in high-iron low-silica regions from 1210 °C to 1260 °C in the same system,<sup>[1]</sup> it was found that equilibration in this region for 8 hours is sufficient for the achievement of equilibrium. Equilibration time required in high-calcium and high-silica regions at high temperatures were also indicated in previous studies.<sup>[48,49,53]</sup> Selected equilibration time for each experiment in the present study are listed in Table V.
2. Homogeneity of phases are examined on different locations throughout the samples and can be verified by the standard deviations of compositions measured (as listed in Table I);

3. Approach to equilibrium from different directions are assessed by selecting starting compositions from: (a) different primary phase fields (Initial mixtures A and B in Table II and plotted in Figure 1; and (b) different total oxygen concentrations in the initial samples made from wustite (Fe<sub>1-y</sub>O) or hematite (Fe<sub>2</sub>O<sub>3</sub>) with the same Fe/(Fe + CaO + SiO<sub>2</sub>) and CaO/SiO<sub>2</sub> ratios where relatively higher amount of Fe<sup>2+</sup> in the slag is expected (Initial mixtures C and D in Table II). It can be seen in Table III that the differences in measured liquid compositions obtained from the different starting mixtures/compositions are within the measurement uncertainty of EPMA. Therefore, it is considered that equilibria have been achieved in these samples.
4. Analysis of reactions taking place is demonstrated through the example of the high-SiO<sub>2</sub> liquid formation in Figure 2. Detailed descriptions of the reactions are shown in Table IV. It should be noted that the reactions e<sub>4</sub> and e<sub>5</sub> are limited by the slow diffusion rate of cations through the highly viscous high-SiO<sub>2</sub> liquid. This results in the retention of SiO<sub>2</sub> particles once encapsulated in the high-SiO<sub>2</sub> liquid, as seen in the microstructure in Figure 2.

### III. RESULTS

Back scattered electron micrographs of typical microstructures of samples obtained in various compositional regions in the “FeO<sub>1.5</sub>”-SiO<sub>2</sub>, CaO-SiO<sub>2</sub> and “FeO<sub>1.5</sub>”-CaO-SiO<sub>2</sub> systems in air, are shown in Figures 3 and 4. The following phases: liquid (Liq), hematite (Fe<sub>2</sub>O<sub>3</sub>), spinel [(Fe,Ca)O·Fe<sub>2</sub>O<sub>3</sub>], lime (CaO), tridymite or cristobalite (SiO<sub>2</sub>), dicalcium ferrite (2CaO·Fe<sub>2</sub>O<sub>3</sub>, C<sub>2</sub>F), pseudo-wollastonite (CaO·SiO<sub>2</sub>, CS), rankinite (3CaO·2SiO<sub>2</sub>, C<sub>3</sub>S<sub>2</sub>), dicalcium silicate (2CaO·SiO<sub>2</sub>, C<sub>2</sub>S), tricalcium silicate (3CaO·SiO<sub>2</sub>, C<sub>3</sub>S) and two immiscible liquids, have been identified in the range of compositions investigated.

Figures 1(a) and 2(g) show an equilibrium microstructure of two immiscible liquids (Fe-rich liquid (Liq1) and Si-rich liquid (Liq2). SiO<sub>2</sub> particles less than < 10 μm in diameter are observed to be encapsulated in the high-SiO<sub>2</sub> liquid. Compositions of this liquid have been carefully measured, avoiding inclusions of the SiO<sub>2</sub> crystals. In Figures 1(a), (b), 2(b), (c), (f) and (h), it can

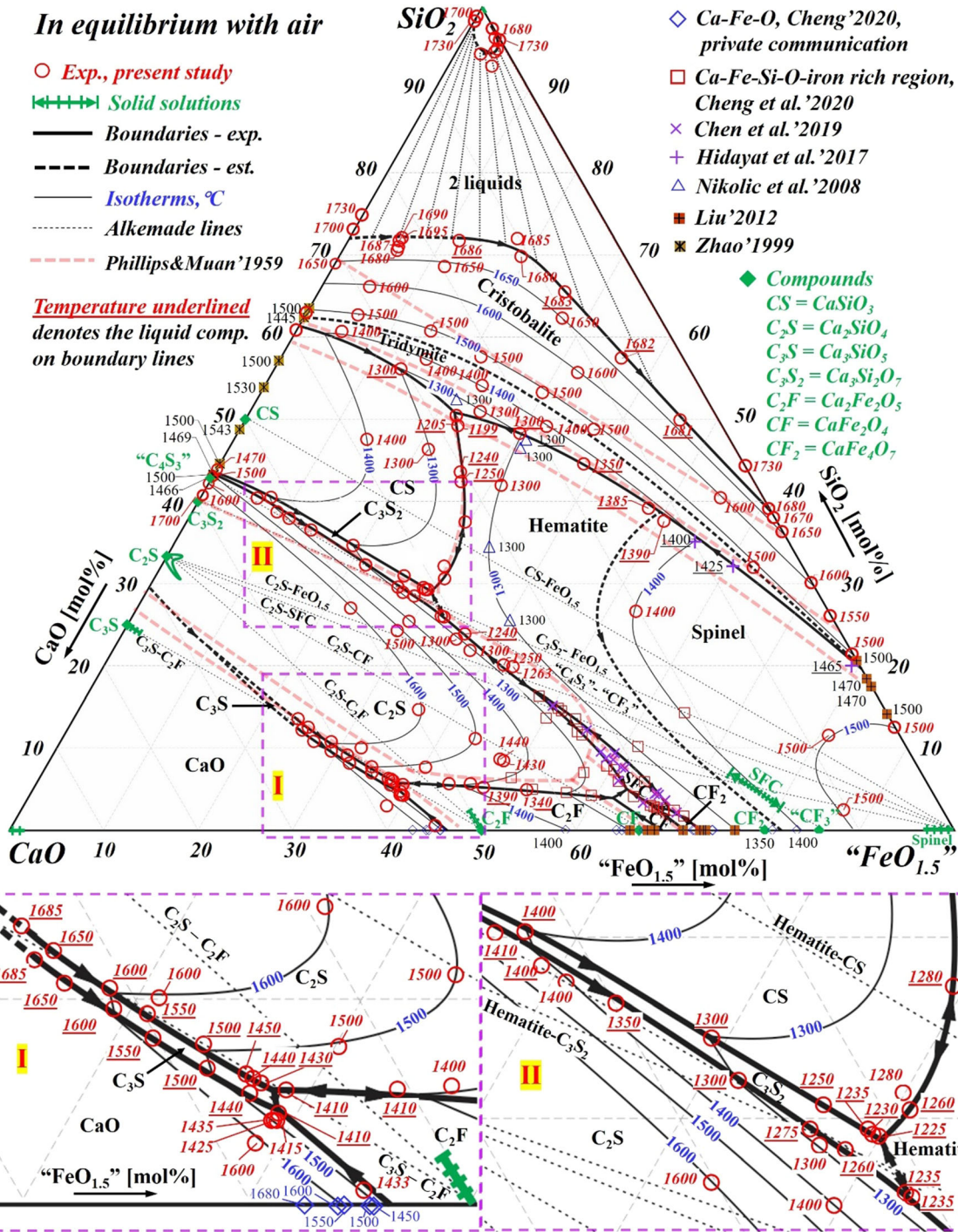


Fig. 5—Proposed liquidus surface of the “FeO<sub>1.5</sub>”-CaO-SiO<sub>2</sub> system in air, with all experimental points from the present study plotted. Composition in mol pct, temperature in °C.

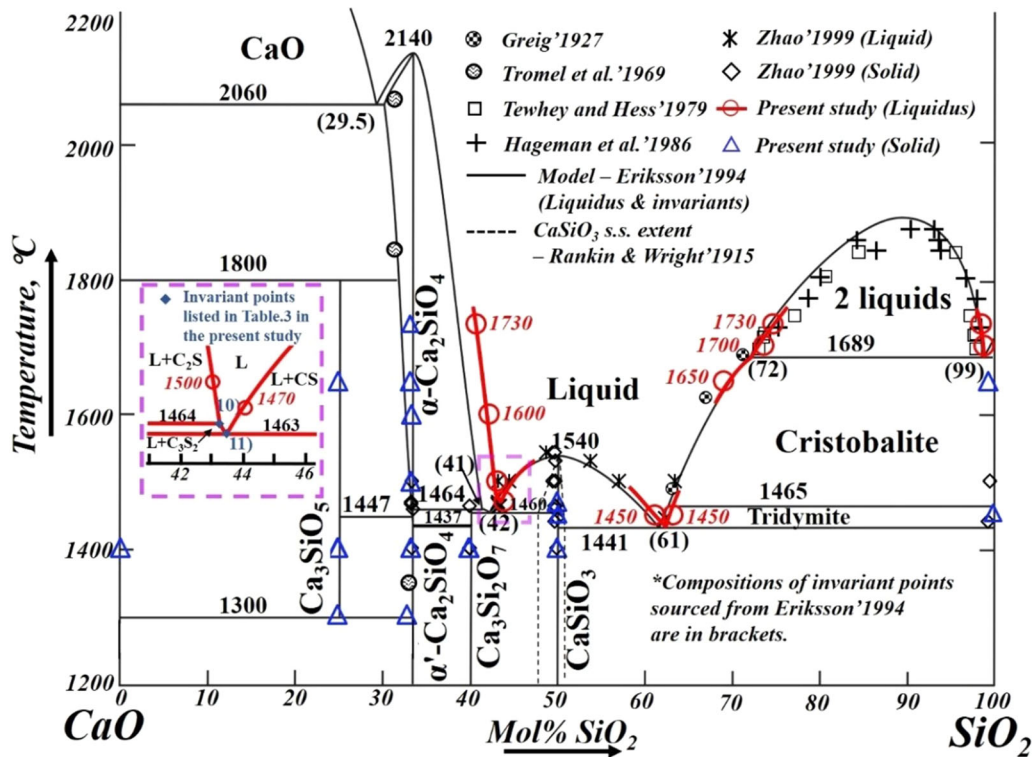


Fig. 6—Results obtained in the present study plotted onto the CaO-SiO<sub>2</sub> binary phase diagram, in comparison with previous studies,<sup>[6,8,13–17]</sup> all invariant points and boundary lines on this diagram are sourced from the thermodynamic assessment by Eriksson *et al.*<sup>[18]</sup> Compositions in mol pct, temperatures in °C.

be seen that micro-crystalline material is present in some parts of the glassy matrix; the micro-crystalline material is an artefact of the quenching process, formed due to high fluidity of the slag or quenching from high equilibration temperature. Measurements of the liquid composition in these samples are taken on the well-quenched, micro-crystalline-free regions with increased probe diameters as described in the experimental methodology. The measured average molar compositions and standard deviations of the measurements of each phase are given in Table V.

It should be noted that measurement of a few solid lime compositions (experiment no. 22, 31, 32, 33, 106, 107 in Table V) shows a relatively low “Old total” (lowest at ~ 67 wt pct). This reflects that hydration of lime has occurred during metallographic preparation or further storage of the sample, this does not affect the Ca/Fe ratio in lime. In few cases (experiment no. 40, 42, 66 in Table V) due to the small size of solid phase (below the interaction volume), no accurate measurements of the solid composition are obtained therefore only the liquid composition is reported.

The proposed liquidus surface in mol pct in the “FeO<sub>1.5</sub>”-CaO-SiO<sub>2</sub> system in air is shown in Figure 5, constructed using experimental data points from Table V obtained in the present study as well as from the studies by previous authors.<sup>[1,2,13,24,29,30,33]</sup> The estimated liquid compositions and temperatures of the invariant points in the “FeO<sub>1.5</sub>”-CaO-SiO<sub>2</sub> system in air, are also summarized in Table VI.

## IV. DISCUSSION

### A. CaO-SiO<sub>2</sub> System in Air

The experimental data obtained for the CaO-SiO<sub>2</sub> system in the present study are plotted on Figure 6, adapted from the calculated diagram by Eriksson *et al.*<sup>[18]</sup> The solids 3CaO·SiO<sub>2</sub>, 2CaO·SiO<sub>2</sub>, 3CaO·2SiO<sub>2</sub> and CaO·SiO<sub>2</sub> measured in the present study in the CaO-SiO<sub>2</sub> system are close to their respective stoichiometric compositions (below the measurement uncertainty of EPMA) within the temperature range investigated. No significant solid solution in α-2CaO·SiO<sub>2</sub> is detected at temperatures up to 1650 °C for C<sub>2</sub>S-C<sub>3</sub>S equilibria. The compositions of the liquid in equilibrium with α-2CaO·SiO<sub>2</sub> obtained in the present study indicate (i) the liquidus in the α-2CaO·SiO<sub>2</sub> primary phase field is higher than the previous assessment by Eriksson *et al.*<sup>[18]</sup> and (ii) the liquidus of 3CaO·2SiO<sub>2</sub> exists in a narrow range of composition in the CaO-SiO<sub>2</sub> system (43.1~43.4 mol pct SiO<sub>2</sub>). The eutectic composition between 3CaO·2SiO<sub>2</sub> and CaO·SiO<sub>2</sub> is close to 43.4 mol pct SiO<sub>2</sub>, slightly higher than the 42.0 mol pct reported by Eriksson *et al.*<sup>[18]</sup> The peritectic composition between 3CaO·2SiO<sub>2</sub> and α-2CaO·SiO<sub>2</sub> is close to 43.1 mol pct SiO<sub>2</sub> which is in good agreement with Zhao’s study.<sup>[13]</sup> The formation temperature of 3CaO·SiO<sub>2</sub> is not obtained in the present study due to the slow rate of solid diffusion. The decomposition temperature of 3CaO·SiO<sub>2</sub> at high temperature (>1800 °C) is also

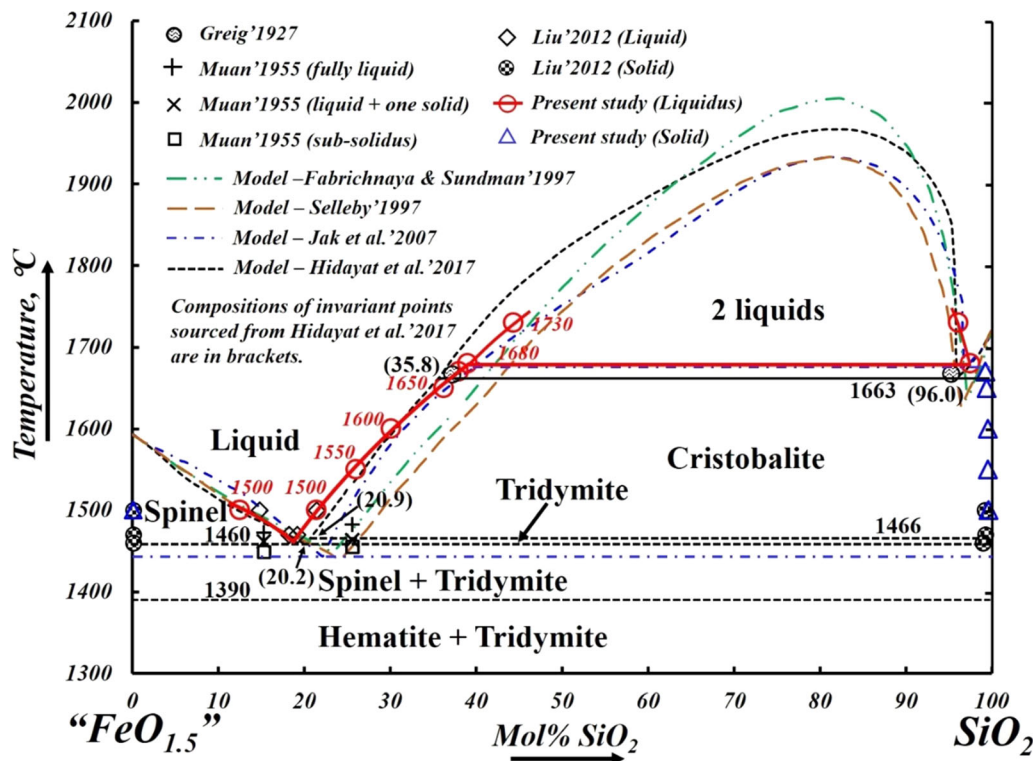


Fig. 7—Results obtained in the present study plotted onto the “FeO<sub>1.5</sub>”-SiO<sub>2</sub> pseudo-binary phase diagram in air (diagram adapted from Hidayat *et al.*<sup>[24]</sup>), in comparison with previous experimental studies<sup>[14,15,19,20]</sup> and thermodynamic models,<sup>[21–24]</sup> all invariant points and boundary lines on this diagram are also sourced from Hidayat *et al.*<sup>[24]</sup> Compositions in mol pct, Temperatures in °C.

not obtained due to the furnace capacity (<1750 °C), therefore they are set out of scope in the present study.

### B. “FeO<sub>1.5</sub>”-SiO<sub>2</sub> System in Air

In the “FeO<sub>1.5</sub>”-SiO<sub>2</sub> system in air (Figure 7), the liquidus in the cristobalite (SiO<sub>2</sub>) primary phase field has been determined between 1550 °C and 1680 °C; the spinel liquidus has been measured at 1500 °C in the present study. Two immiscible liquids are observed at 1680 °C in the SiO<sub>2</sub>-rich region. These results indicate: (i) a slightly lower SiO<sub>2</sub> concentration in liquid comparing with the model by Hidayat *et al.*<sup>[24]</sup> and good agreement with the experimental study by Liu<sup>[20]</sup> when in equilibrium with cristobalite at temperatures below 1600 °C; (ii) a higher monotectic temperature (1671 °C to 1680 °C) comparing to the 1663 °C reported by Hidayat *et al.*<sup>[24]</sup> These differences arise because of the insufficient experimental data available during the time when the thermodynamic assessment in this system by Hidayat *et al.*<sup>[24]</sup> was carried out. The apparent solubility of 1.4 to 1.7 wt pct of Fe<sub>2</sub>O<sub>3</sub> (1.0 to 1.2 mol pct of FeO<sub>1.5</sub>) in cristobalite initially measured by EPMA, is close to Liu’s result.<sup>[20]</sup> It has further been corrected to approximately 0.5 to 0.9 wt pct (0.3 to 0.7 mol pct) in the present study by subtracting the secondary X-ray fluorescence of Fe from the adjacent slag phase. Further research on minimizing the secondary X-ray

fluorescence during measurement is required to more accurately characterize the true chemical solubility of Fe in cristobalite.

### C. “FeO<sub>1.5</sub>”-CaO-SiO<sub>2</sub> System in Air

The liquidus surface of the “FeO<sub>1.5</sub>”-CaO-SiO<sub>2</sub> system in air, with all invariant points summarized, is constructed in Figure 8. The results in the iron-rich regions were reported and discussed in a previous publication.<sup>[2]</sup> The isotherms above 1700 °C in the α-2CaO·SiO<sub>2</sub> and CaO primary phase fields are estimated from the public FactSage database.<sup>[23,55,56]</sup> The wide range of compositions and temperatures investigated in the present study indicate a number of features in the system that is different from / were not reported in previous publications.

A narrow shape of the 3CaO·SiO<sub>2</sub> primary phase field has been determined from equilibrium with α-C<sub>2</sub>S and CaO up to 1685 °C. The width of the 3CaO·SiO<sub>2</sub> primary phase field is narrower than the previous interpretation by Phillips and Muan.<sup>[32]</sup> The temperature of the invariant point between Liquid-C<sub>3</sub>S-CaO-C<sub>2</sub>S is estimated to be at approximately 1960 °C. This value of the temperature at this invariant point is recently reported in the thermodynamic assessments of other CaO-MeO-SiO<sub>2</sub> systems: 1986 °C in CaO-ZnO-SiO<sub>2</sub> system<sup>[54]</sup> and 2000 °C in CaO-PbO-SiO<sub>2</sub> system.<sup>[57]</sup> The existence of this invariant point and



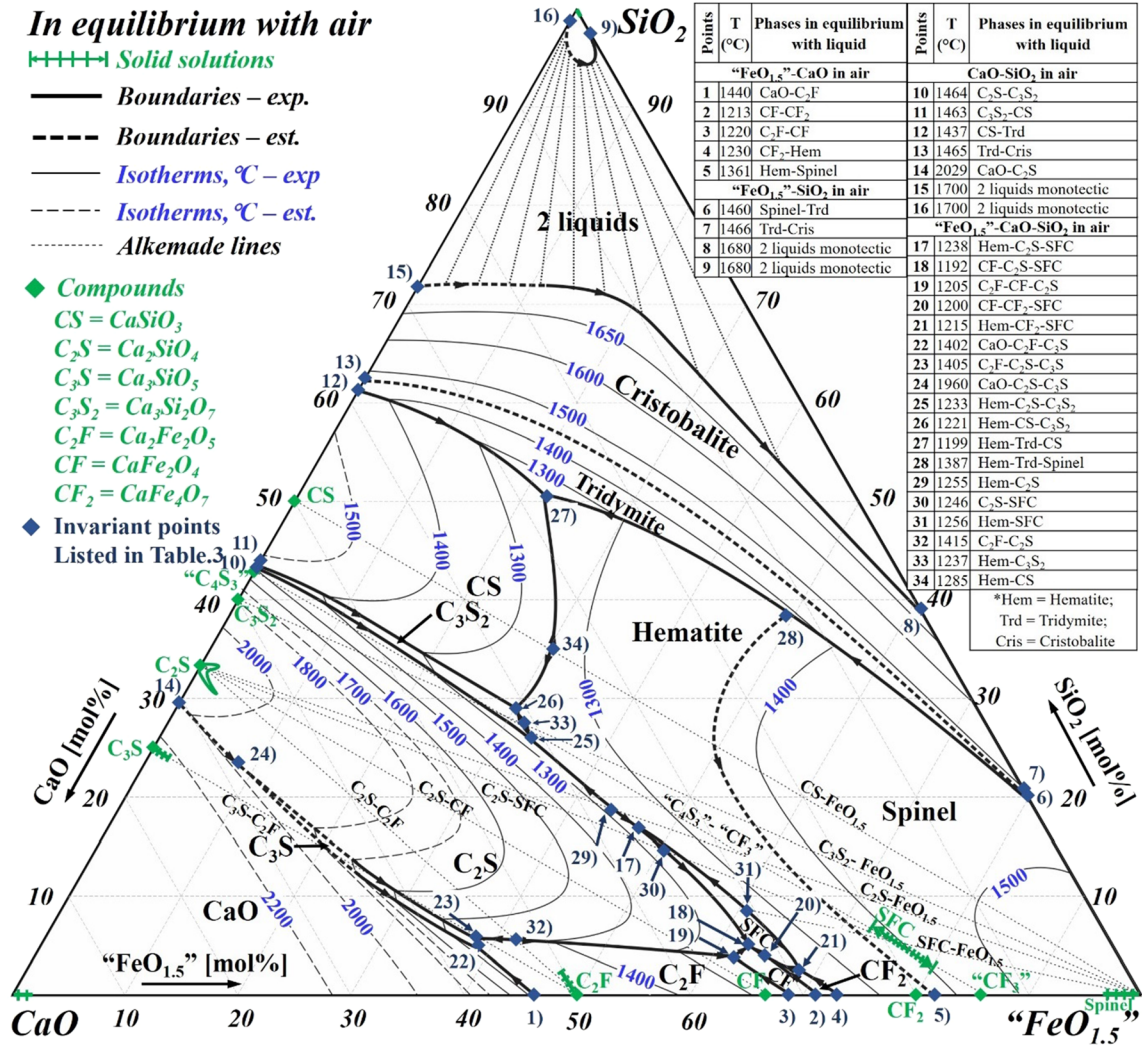


Fig. 8—Proposed liquidus surface of the “FeO<sub>1.5</sub>”-CaO-SiO<sub>2</sub> system in air, invariant points are plotted and listed in detail in Table VI. Compositions in mol pct. Temperatures in °C.

its temperature is not verified in the present study due to the limited temperature attainable using of the present furnace.

The solubility of Fe in 2CaO·SiO<sub>2</sub>, 3CaO·SiO<sub>2</sub> (after correcting for secondary X-ray fluorescence) and solubility of Si in C<sub>2</sub>F and the tie-lines in these primary phase fields are given in Figure 9. The data showing the equilibrium of liquid-2CaO·SiO<sub>2</sub> with SFC are sourced from a previous publication.<sup>[2]</sup> In the present study, up to 2.5 mol pct of SiO<sub>2</sub> is observed in Ca<sub>2</sub>Fe<sub>2</sub>O<sub>5</sub>. Approximately 1.0 mol pct of Fe as FeO<sub>1.5</sub> is observed in 3CaO·SiO<sub>2</sub> and this value appears to be insensitive to the equilibration temperature between 1400 °C and 1685 °C.

The solubility of Fe as FeO<sub>1.5</sub> in 2CaO·SiO<sub>2</sub> is found to be less than 2.8 mol pct. The 2CaO·SiO<sub>2</sub> compositions at different temperature ranges (from 1193 °C to 1685 °C) and the liquid-2CaO·SiO<sub>2</sub> tie-lines measured in the present study are plotted in Figure 10. It is found that the 2CaO·SiO<sub>2</sub> in exp. 55, 92, 103 through 110 and

120 in Table V have exhibited distinctively high Fe solubility (>1.5 mol pct FeO<sub>1.5</sub>) with Fe cation substituting Si cation while CaO concentration remaining constant at its stoichiometric composition 66.7 mol pct. It is expected that if the Fe oxide solubility in 2CaO·SiO<sub>2</sub> follows the substitution reactions: (i) Ca<sup>2+</sup> ↔ Fe<sup>2+</sup>, the 2CaO·SiO<sub>2</sub> compositions would lie on the C<sub>2</sub>S-F<sub>2</sub>S join; or if (ii) Si<sup>4+</sup> + Ca<sup>2+</sup> ↔ 2Fe<sup>3+</sup>, the 2CaO·SiO<sub>2</sub> compositions would lie on the C<sub>2</sub>S-CF join. Some of the measured compositions of the 2CaO·SiO<sub>2</sub> in the present study with relatively low Fe in 2CaO·SiO<sub>2</sub> (< 1.0 mol pct FeO<sub>1.5</sub>) appear to agree with the Ca<sup>2+</sup> ↔ Fe<sup>2+</sup> substitution, while the compositions of the 2CaO·SiO<sub>2</sub> with high Fe solubility (> 1.5 mol pct FeO<sub>1.5</sub>) are found to lie on the C<sub>2</sub>S-“C<sub>4</sub>F” join (constant CaO concentrations, see Figure 11), which does not agree with the substitution reaction Si<sup>4+</sup> + Ca<sup>2+</sup> ↔ 2Fe<sup>3+</sup>. It is also noticed that the high Fe solubility in 2CaO·SiO<sub>2</sub> takes place only when the composition of the liquid in equilibrium satisfies the following numerical expression:

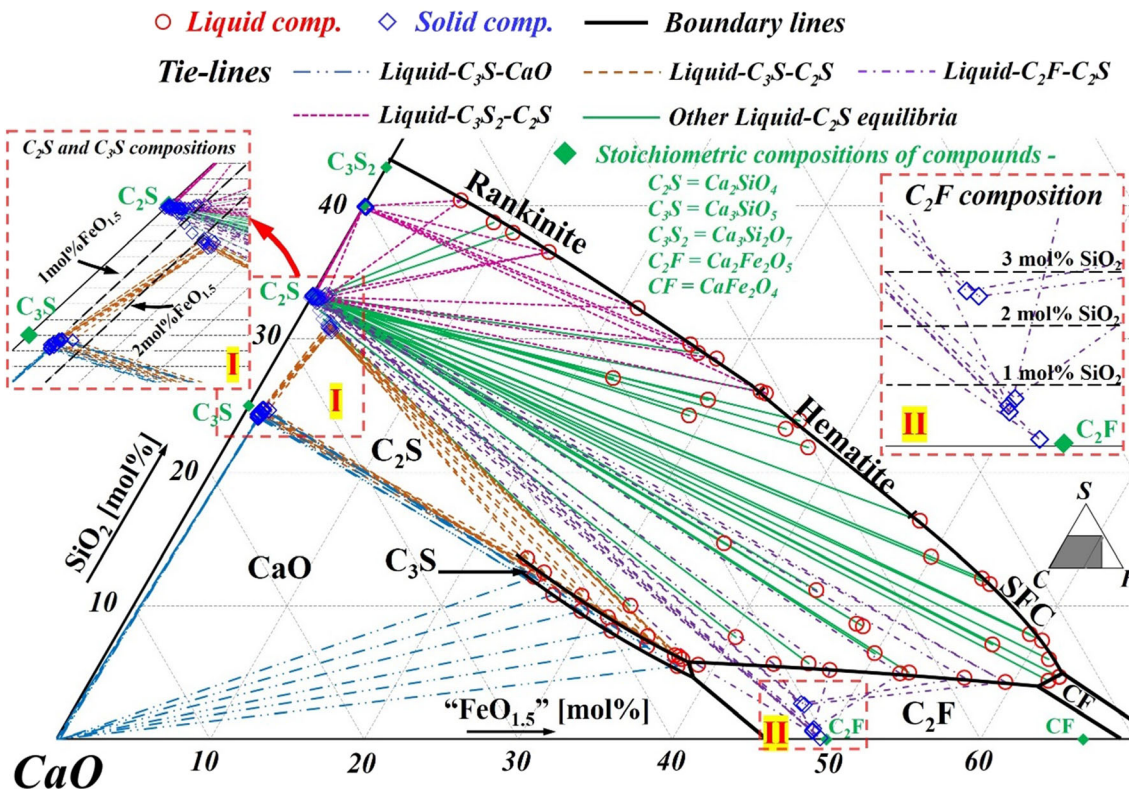


Fig. 9—Tie-lines connecting compositions of liquid and solids in the  $C_2S$  and  $C_3S$  primary phase fields to illustrating the limits of the solid solutions in  $C_2S$ ,  $C_3S$  and  $C_2F$  in the “ $FeO_{1.5}$ ”- $CaO$ - $SiO_2$  system in air.

$$\text{Mol pct } SiO_2 \text{ in slag} + 0.667$$

$$* \text{ Mol pct } FeO_{1.5} \text{ in slag} < 33.3$$

The formula graphically indicates the higher-calcium side of the  $2CaO \cdot SiO_2$  ( $C_2S$ )- $2CaO \cdot Fe_2O_3$  ( $C_2F$ ) join in the “ $FeO_{1.5}$ ”- $CaO$ - $SiO_2$  pseudo-ternary diagram (see Figure 12). This is confirmed by the experiments on both sides on the  $C_2S$ - $C_2F$  join at the same temperatures (exp. 92/93 at 1410 °C, exp. 107/58 at 1500 °C and exp. 105/53 at 1600 °C). Whether the difference in solubility behavior is an indication of different polymorphism of  $2CaO \cdot SiO_2$  ( $\alpha$  and  $\alpha'$ ), is to be further confirmed. Fe (as mol pct “ $FeO_{1.5}$ ”) measured in  $2CaO \cdot SiO_2$  in the present study is plotted with respect to temperatures in Figure 13, with a maximum solubility found to be at 2.6 mol pct  $FeO_{1.5}$  at 1500 °C.

The primary phase field of the rankinite in the “ $FeO_{1.5}$ ”- $CaO$ - $SiO_2$  system in air is determined up to 1410 °C and is found to be narrower in width compared to the previous version of the diagram constructed by Phillips and Muan.<sup>[32]</sup> No significant solubility of Fe is observed in rankinite ( $3CaO \cdot 2SiO_2$ ) and pseudo-wollastonite ( $CaO \cdot SiO_2$ ).

In the high- $SiO_2$  region, new experimental data have been obtained in the primary phase fields of tridymite and cristobalite from 1300 °C to 1690 °C. These demonstrate the non-linear behavior of the liquidus isotherms between the limiting  $CaO$ - $SiO_2$  and “ $FeO_{1.5}$ ”- $SiO_2$  binaries,

behavior that becomes more pronounced with increasing temperature. The temperature of the tridymite-cristobalite transition has not been directly determined and accepted from the FactSage database predictions<sup>[23,55,56]</sup> as 1465 °C. The liquid immiscibilities in the high- $SiO_2$  region and the associated tie lines have been measured at temperatures between 1680 °C and 1686 °C for a wide range of Ca/Fe ratios. It was found that the second  $SiO_2$ -rich liquid was not formed at temperatures up to 1695 °C (exp. 34 in Table V) in the regions with the high Ca/Fe ratio, indicating the monotectic temperature in the  $CaO$ - $SiO_2$  binary system is higher than 1695 °C, and is estimated to be 1700 °C in the present study. This is in good agreement with the temperature reported by Greig *et al.*<sup>[14]</sup> and Tewhey *et al.*<sup>[16]</sup> (1695 °C to 1700 °C).

The systematic measurement of phase compositions, phase boundaries and invariant points in the “ $FeO_{1.5}$ ”- $CaO$ - $SiO_2$  system in air undertaken in the present study have enabled important additions to, and refinement of, the phase diagram presented previously by Phillips and Muan.<sup>[32]</sup> In particular, the following features are pointed out. (i) The saddle point on the  $C_2S$ - $C_2F$  univariant line (point [32] in Figure 8), has been confirmed by experiments 83 and 84 in Table V; (ii) the saddle point on the Rankinite-Hematite univariant line (point [33] in Figure 8), has been estimated by the temperatures of the invariant points liquid-Rankinite-Hematite- $C_2S$  (point [25]) and liquid-Rankinite-Hematite- $C_3S$  (point [26]); (iii) the eutectic temperature for liquid-Tridymite-Hematite- $C_3S$  (point [27])

**Table VI. Estimated Temperatures and Liquid Compositions of Invariant and Saddle Points for the System “FeO<sub>1.5</sub>”-CaO-SiO<sub>2</sub> in Air Listed in Figs. 5 and 6, Binary Invariant Points are Also Evaluated Based on the Experimental Data in the Present Study (PS) and Previous Publications.<sup>[2,13,18,20,24,29,30]</sup> Hem = Hematite, Trd = Tridymite, Cris = Cristobalite, SFC = Silico-ferrite of Calcium Solid Solution**

| Points   | Temp. (°C) | Estimated/Reported (°C) | Phases in Equilibrium with Liquid                  | Liquid Composition (Mol Pct) |                       |                  | Liquid Composition (Wt Pct) |                                   |                  | References |       |
|--|------------|-------------------------|--|------------------------------|-----------------------|------------------|-----------------------------|-----------------------------------|------------------|------------|-------|
|  |            |                         |  | CaO                          | “FeO <sub>1.5</sub> ” | SiO <sub>2</sub> | CaO                         | “Fe <sub>2</sub> O <sub>3</sub> ” | SiO <sub>2</sub> |            | C/S   |
| <i>Pseudo-binary invariant points</i>                    |            |                         |  |                              |                       |                  |                             |                                   |                  |            |       |
| <i>“FeO<sub>1.5</sub>”-CaO system in air</i>             |            |                         |  |                              |                       |                  |                             |                                   |                  |            |       |
| 1  | —          | 1440                    | CaO-C <sub>2</sub> F                               | 53.8                         | 46.2                  | 0.0              | 45.0                        | 55.0                              | 0.0              | —          | 29    |
| 2  | 1211–1214  | 1213                    | CF-CF <sub>2</sub>                                 | 31.3                         | 68.7                  | 0.0              | 24.2                        | 75.8                              | 0.0              | —          | 30    |
| 3  | 1215–1225  | 1220                    | C <sub>2</sub> F-CF                                | 28.9                         | 71.1                  | 0.0              | 22.2                        | 77.8                              | 0.0              | —          |       |
| 4  | 1230–1235  | 1230                    | CF <sub>2</sub> -Hem                               | 27.0                         | 73.0                  | 0.0              | 20.6                        | 79.4                              | 0.0              | —          |       |
| 5  | —          | 1361                    | hem-spinel   | 18.3                         | 81.7                  | 0.0              | 13.6                        | 86.4                              | 0.0              | —          | 29,30 |
| <i>“FeO<sub>1.5</sub>”-SiO<sub>2</sub> system in air</i> |            |                         |  |                              |                       |                  |                             |                                   |                  |            |       |
| 6  | —          | 1460                    | spinel-Trd   | 0.0                          | 79.8                  | 20.2             | 0.0                         | 84.0                              | 16.0             | —          | 20,24 |
| 7  | —          | 1466                    | Trd-Cris   | 0.0                          | 79.1                  | 20.9             | 0.0                         | 83.5                              | 16.5             | —          |       |
| 8  | 1671–1680  | 1680                    | 2 liquids  | 0.0                          | 60.9                  | 39.1             | 0.0                         | 67.5                              | 32.5             | —          | PS    |
| 9  | 1671–1680  | 1680                    | 2 liquids  | 0.0                          | 2.4                   | 97.5             | 0.0                         | 3.2                               | 96.8             | —          |       |
| <i>CaO-SiO<sub>2</sub> system in air</i>                 |            |                         |  |                              |                       |                  |                             |                                   |                  |            |       |
| 10   | —          | 1464                    | C <sub>2</sub> S-C <sub>3</sub> S <sub>2</sub>     | 56.9                         | 0.0                   | 43.1             | 55.2                        | 0.0                               | 44.8             | 1.2        | 13    |
| 11   | —          | 1463                    | C <sub>3</sub> S <sub>2</sub> -CS                  | 56.6                         | 0.0                   | 43.4             | 54.9                        | 0.0                               | 45.1             | 1.2        |       |
| 12   | —          | 1437                    | CS-Trd   | 38.7                         | 0.0                   | 61.3             | 37.1                        | 0.0                               | 62.9             | 0.6        |       |
| 13   | —          | 1465                    | Trd-Cris   | 37.5                         | 0.0                   | 62.5             | 35.9                        | 0.0                               | 64.1             | 0.6        | 18    |
| 14   | —          | 2029                    | CaO-C <sub>2</sub> S                               | 70.4                         | 0.0                   | 29.6             | 68.9                        | 0.0                               | 31.1             | 2.2        | 54    |
| 15   | —          | 1700                    | 2 liquids  | 28.2                         | 0.0                   | 71.8             | 26.8                        | 0.0                               | 73.2             | 0.4        | 14,17 |
| 16   | —          | 1700                    | 2 liquids  | 1.2                          | 0.0                   | 98.8             | 1.1                         | 0.0                               | 98.9             | 0.0        |       |
| <i>Pseudo-ternary invariant points</i>                   |            |                         |  |                              |                       |                  |                             |                                   |                  |            |       |
| 17   | 1236–1240  | 1238                    | hem-C <sub>2</sub> S-SFC                           | 36.1                         | 47.0                  | 16.9             | 29.8                        | 55.2                              | 14.9             | 2.0        | 2     |
| 18   | 1190–1193  | 1192                    | CF-C <sub>2</sub> S-SFC                            | 32.3                         | 62.6                  | 5.1              | 25.5                        | 70.2                              | 4.3              | 5.9        |       |
| 19   | 1203–1209  | 1205                    | C <sub>2</sub> F-CF-C <sub>2</sub> S               | 34.2                         | 62.0                  | 3.8              | 27.0                        | 69.8                              | 3.2              | 8.4        |       |
| 20   | 1199–1203  | 1200                    | CF-CF <sub>2</sub> -SFC                            | 31.4                         | 64.6                  | 4.0              | 24.6                        | 72.0                              | 3.3              | 7.4        |       |
| 21   | 1213–1217  | 1215                    | hem-CF <sub>2</sub> -SFC                           | 29.1                         | 68.4                  | 2.5              | 22.5                        | 75.4                              | 2.1              | 10.9       |       |
| 22   | 1401–1409  | 1402                    | CaO-C <sub>2</sub> F-C <sub>3</sub> S              | 56.2                         | 38.8                  | 5.0              | 48.1                        | 47.3                              | 4.6              | 10.5       | PS    |
| 23   | 1401–1409  | 1405                    | C <sub>2</sub> F-C <sub>2</sub> S-C <sub>3</sub> S | 56.0                         | 38.1                  | 5.9              | 48.0                        | 46.5                              | 5.4              | 8.9        |       |
| 24   | —          | 1960                    | CaO-C <sub>2</sub> S-C <sub>3</sub> S              | 68.2                         | 8.3                   | 23.5             | 64.8                        | 11.2                              | 23.9             | 2.7        |       |
| 25   | 1230–1235  | 1233                    | hem-C <sub>2</sub> S-C <sub>3</sub> S <sub>2</sub> | 41.0                         | 33.0                  | 26.0             | 35.4                        | 40.6                              | 24.0             | 1.5        |       |
| 26   | 1221–1224  | 1221                    | hem-CS-C <sub>3</sub> S <sub>2</sub>               | 40.9                         | 30.1                  | 29.0             | 35.6                        | 37.3                              | 27.1             | 1.3        |       |
| 27   | 1198–1204  | 1199                    | hem-Trd-CS   | 27.4                         | 22.1                  | 50.5             | 24.3                        | 27.9                              | 47.9             | 0.5        |       |
| 28   | 1386–1389  | 1387                    | hem-Trd-spinel                                     | 12.3                         | 49.3                  | 38.4             | 9.9                         | 56.8                              | 33.3             | 0.3        |       |
| <i>Saddle points on boundary lines</i>                   |            |                         |  |                              |                       |                  |                             |                                   |                  |            |       |
| 29   | 1250–1260  | 1255                    | hem-C <sub>2</sub> S                               | 37.6                         | 43.7                  | 18.7             | 31.4                        | 51.9                              | 16.7             | 1.9        | 2     |
| 30   | 1245–1250  | 1246                    | C <sub>2</sub> S-SFC                               | 35.0                         | 50.4                  | 14.6             | 28.6                        | 58.6                              | 12.8             | 2.2        |       |
| 31   | 1250–1257  | 1256                    | hem-SFC  | 30.7                         | 60.8                  | 8.5              | 24.3                        | 68.5                              | 7.2              | 3.4        |       |
| 32   | 1411–1420  | 1415                    | C <sub>2</sub> F-C <sub>2</sub> S                  | 52.6                         | 41.8                  | 5.6              | 44.5                        | 50.4                              | 5.1              | 8.8        | PS    |
| 33   | 1236–1240  | 1237                    | hem-C <sub>3</sub> S <sub>2</sub>                  | 40.9                         | 31.6                  | 27.5             | 35.5                        | 39.0                              | 25.5             | 1.4        |       |
| 34   | 1281–1290  | 1285                    | hem-CS   | 34.6                         | 30.4                  | 35.0             | 30.0                        | 37.5                              | 32.5             | 0.9        |       |

has been determined to be 1199 °C by experiments 108 and 109 in Table V; (iv) the transition temperature (point [28]) between spinel and hematite in equilibrium with liquid and tridymite has been determined to be between 1386 °C and 1389 °C by experiments 63 and 66 in Table V, which is higher than the transition temperature (1361 °C by Hidayat *et al.*,<sup>[29]</sup> point [5]) on the “FeO<sub>1.5</sub>”-CaO pseudo-binary system in air, indicating the presence of CaO stabilizes spinel over hematite.

In summary, present experimental study has produced a comprehensive and systematic phase equilibria dataset for the “FeO<sub>1.5</sub>”-CaO-SiO<sub>2</sub> system in air, with key regions in the “FeO<sub>1.5</sub>”-SiO<sub>2</sub> and CaO-SiO<sub>2</sub> sub-systems in air evaluated. These data are essential for a wide range of cement, refractory, ferrous and non-ferrous industrial processes, and provides valuable new data that can be used to optimize the thermodynamic databases of these systems.

○ *Liquid comp.*    ◇ *Solid comp.*    — *Tie-lines*  
*(label denotes temperature in °C, mol% Fe in C<sub>2</sub>S)*  
 - - - *Estimated C<sub>2</sub>S solution at various temperatures*

◆ *Stoichiometric compositions of compounds -*

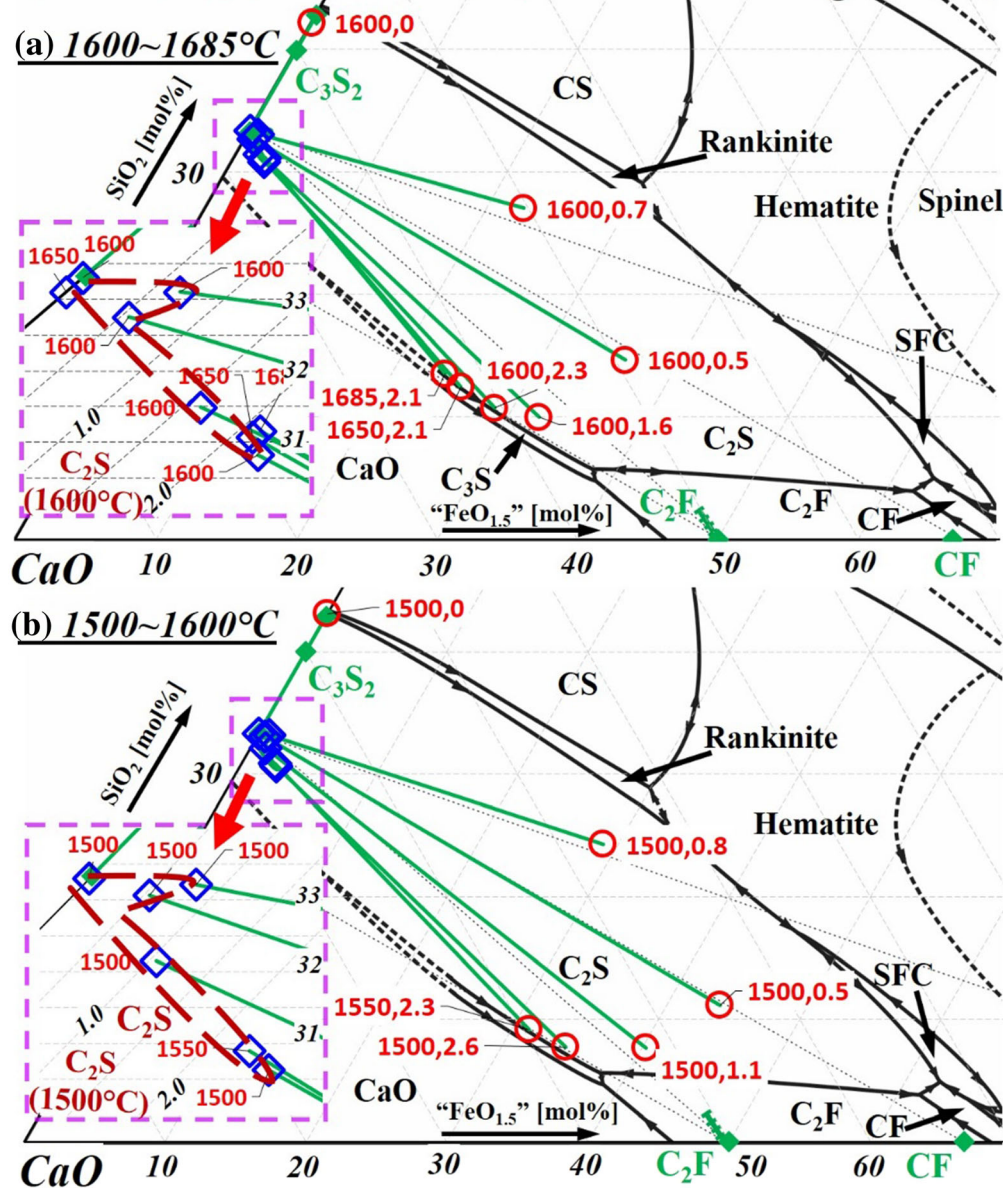
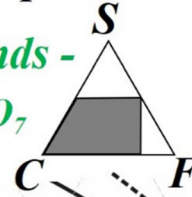
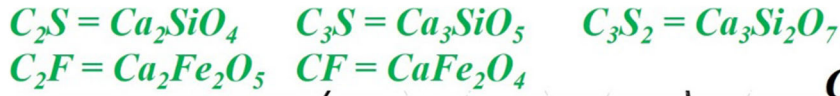


Fig. 10—Estimated 2CaO-SiO<sub>2</sub> solid solution extents at different temperatures (brown dash line) in the “FeO<sub>1.5</sub>”-CaO-SiO<sub>2</sub> system in air, temperature in °C, number next to temperature denotes mol pct of FeO<sub>1.5</sub> measured in 2CaO-SiO<sub>2</sub> after correcting for secondary X-ray fluorescence, (a) 1600–1685 °C, (b) 1500–1600 °C, (c) 1400–1500 °C, (d) 1300–1400 °C, (e) 1190–1300 °C (Color figure online).



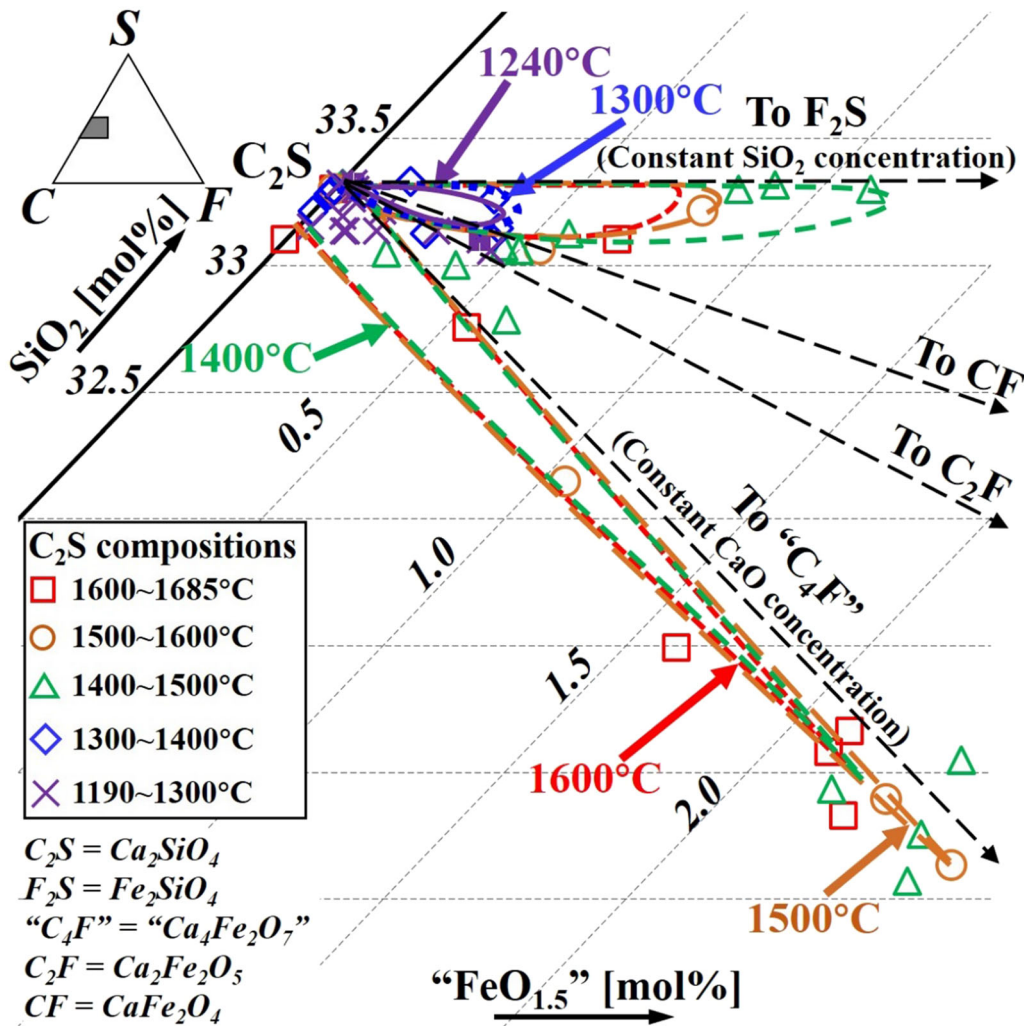


Fig. 11—Limits of 2CaO·SiO<sub>2</sub> solid solutions at 1240 °C, 1300 °C, 1400 °C, 1500 °C and 1600 °C constructed based on the 2CaO·SiO<sub>2</sub> compositions listed in Table V.

## V. CONCLUSIONS

New experimentally-measured phase equilibria information in the FeO-Fe<sub>2</sub>O<sub>3</sub>-CaO-SiO<sub>2</sub>, CaO-SiO<sub>2</sub> and FeO-Fe<sub>2</sub>O<sub>3</sub>-SiO<sub>2</sub> systems in air has been obtained. The measurements have been made for temperatures between 1190 °C and 1700 °C, and for multi-phase equilibria in the primary phase fields of hematite (Fe<sub>2</sub>O<sub>3</sub>), spinel [(Fe,Ca)O·Fe<sub>2</sub>O<sub>3</sub>], lime (CaO), tridymite or cristobalite (SiO<sub>2</sub>), dicalcium ferrite (2CaO·Fe<sub>2</sub>O<sub>3</sub>, C<sub>2</sub>F), pseudo-wollastonite (CaO·SiO<sub>2</sub>, CS), Rankinite (3CaO·2SiO<sub>2</sub>, C<sub>3</sub>S<sub>2</sub>), dicalcium silicate (2CaO·SiO<sub>2</sub>, C<sub>2</sub>S), tricalcium silicate (3CaO·SiO<sub>2</sub>, C<sub>3</sub>S) and two immiscible liquids. The studies have provided important new data on liquidus isotherms, univariant and invariant equilibria in this system.

Major improvements from the present study include the confirmations of the following: (i) liquidus of C<sub>2</sub>S, tridymite, cristobalite and two liquids miscibility gap in the CaO-SiO<sub>2</sub> system and liquidus of tridymite, cristobalite and two liquids miscibility gap in the “Fe<sub>2</sub>O<sub>3</sub>”-SiO<sub>2</sub> system in air at temperatures up to 1730 °C; (ii) primary phase fields of C<sub>3</sub>S, C<sub>2</sub>S and C<sub>3</sub>S<sub>2</sub> in the lime-rich region, primary phase fields of hematite and spinel in the iron-rich region in the “Fe<sub>2</sub>O<sub>3</sub>”-CaO-SiO<sub>2</sub> system in air; (iii) primary phase fields of tridymite, cristobalite and compositions of the two immiscible liquids in the high silica region up to 1690 °C in the “Fe<sub>2</sub>O<sub>3</sub>”-CaO-SiO<sub>2</sub> system in air, where no previous experimental data were available; and (iv) solubilities of iron oxide in the dicalcium silicate, tricalcium silicate, lime, tridymite and cristobalite, with the corrections of

**Recalculated compositions of liquids in equilibrium with  $C_2S$  in Table.2:**

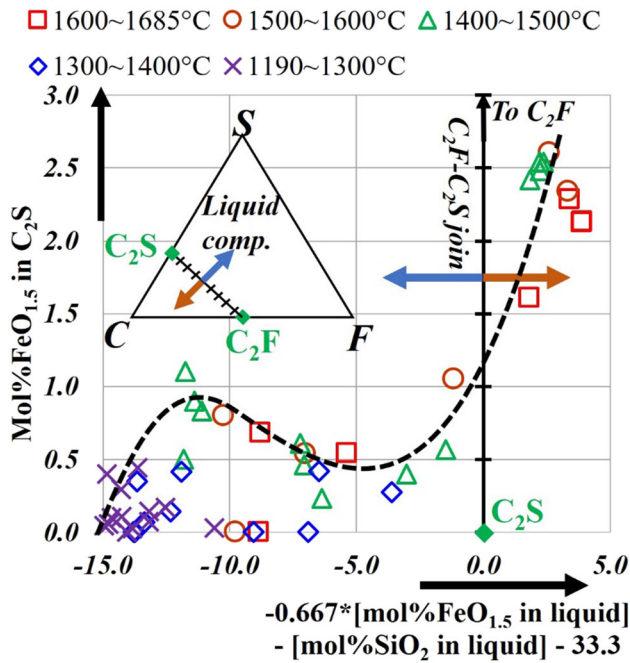


Fig. 12—Solubility of Fe (as mol pct “ $FeO_{1.5}$ ”) in  $2CaO\cdot SiO_2$  plotted against the respective liquid composition in equilibrium. The liquid compositions are recalculated in order to illustrate the location relative to the  $2CaO\cdot SiO_2$  ( $C_2S$ )-  $2CaO\cdot Fe_2O_3$  ( $C_2F$ ) join in the “ $FeO_{1.5}$ ”- $CaO\cdot SiO_2$  pseudo-ternary diagram.

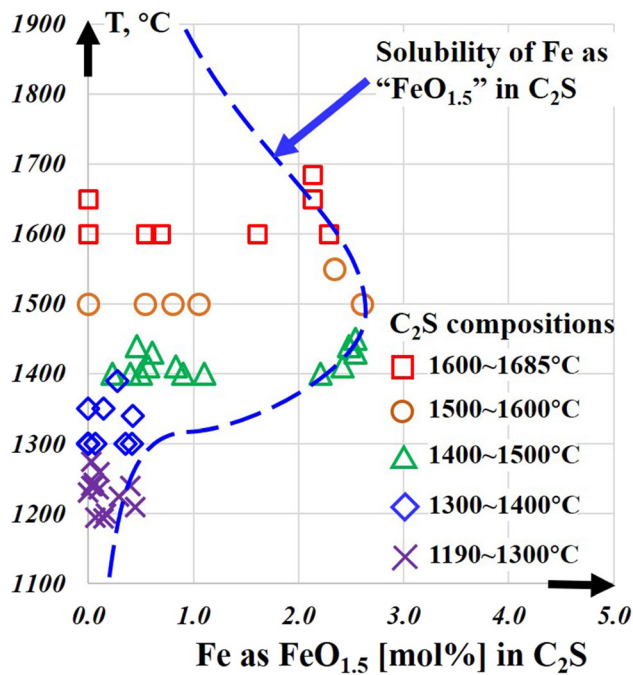


Fig. 13—Maximum solubility of Fe (as mol pct “ $FeO_{1.5}$ ”) in  $2CaO\cdot SiO_2$  observed in the present study at different temperatures (in °C) in air.

secondary fluorescence applied. The measurements obtained in the present study have helped to provide a more complete and more accurate description of the multi-components Fe-Ca-Si-O-Al-Mg-Cu-S system directly relevant to applications in the cement, the ferrous and non-ferrous metallurgical industries.

### ACKNOWLEDGMENTS

The authors would like to acknowledge the Australian Research Council Linkage Program and Altonorte Glencore, Atlantic Copper, Aurubis, Olympic Dam Operation BHP Billiton, Kazzinc Glencore, PASAR Glencore, Outotec Oy (Espoo), Anglo American Platinum, Umicore, and Kennecott Rio Tinto for financial support to enable this research to be carried out, and the Centre for Microscopy and Microanalysis, at the University of Queensland for providing electron microscope facilities and the scientific and technical assistance, and to Mr. Michael Booth, Mr. Kade Parascos, Ms. Marina Chernishova and Ms. Suping Huang for assistance in experimental work.

### REFERENCES

1. J. Chen, M. Shevchenko, P.C. Hayes, and E. Jak: *ISIJ Int.*, 2019, vol. 59, pp. 795–804.
2. S. Cheng, M. Shevchenko, Peter C. Hayes and E. Jak, *Metall. Mater. Trans. B*, 2019, vol. 51, pp. 1587–1602.
3. J. Chen, M. Shevchenko, P. Hayes, and E. Jak: *ISIJ Int.*, 2019, vol. 59, pp. 805–09.
4. S. Cheng, M. Shevchenko, P.C. Hayes, and E. Jak: *Experimental Phase Equilibria Studies in the  $FeO\text{-}Fe_2O_3\text{-}CaO\text{-}Al_2O_3$  System in Air*, PYROSEARCH, The University of Queensland, Private communication, 2020.
5. J. Chen, S. Cheng, M. Shevchenko, P.C. Hayes, and E. Jak: *Metall. Mater. Trans. B*, 2021, <https://doi.org/10.1007/s11663-020-02035-z>.
6. G.A. Rankin and F.E. Wright, *Am. J. Sci.*, (4th series), 1915, vol. 39, pp. 1–79.
7. E.F. Osborn: *J. Am. Ceram. Soc.*, 1943, vol. 26, pp. 321–32.
8. G. Tromel, W. Fix, and R. Heinke: *Tonindustrie-Zeitung und Keramische Rundschau*, 1969, vol. 93, pp. 1–8.
9. S.L. Meyers: *Rock Products*, 1930, vol. 33, pp. 78–79.
10. E.T. Carlson: *Rock Products*, 1931, vol. 34, pp. 52–56.
11. J. Zawadski and J. Gotlied, *Bull. Int. Acad. Polon. Sci. Classe Sci. Math. Nat. Ser. A*, 1948, vol. Ser. A, pp. 32–34.
12. J.H. Welch and W. Gutt: *J. Am. Ceram. Soc.*, 1959, vol. 42, pp. 11–15.
13. B. Zhao, *Phase Equilibria for Copper Smelting and Lead/Zinc Reduction Slags*. Ph.D. Thesis, The University of Queensland, 1999.
14. J.W. Greig, *Am. J. Sci.*, 5th Ser., 1927, vol. 13, pp. 1–44.
15. J.W. Greig, *Am. J. Sci.*, 5th Ser., 1927, vol. 13, pp. 133–54.
16. J.D. Tewhey and P.C. Hess: *Phys. Chem. Glasses*, 1979, vol. 20, pp. 41–53.
17. V.B.M. Hageman, G.J.K. Van den Berg, H.J. Janssen, and H.A.J. Oonk: *Phys. Chem. Glasses*, 1986, vol. 27, pp. 100–06.
18. G. Eriksson, P. Wu, M. Blander, and A.D. Pelton: *Can. Metall. Q.*, 1994, vol. 33, pp. 13–21.
19. A. Muan: *Trans. Metall. Soc. AIME*, 1955, vol. 203, p. 965.
20. X.G. Liu: *Experimental Phase Equilibria Studies in Oxide Systems for Copper Smelting Slags*, Thesis, PYROSEARCH, University of Queensland, Australia, MPhil, 2012.
21. O.B. Fabrichnaya and B. Sundman: *Geochim. Cosmochim. Acta*, 1997, vol. 61, pp. 4539–55.

22. M. Selleby: *Metall. Trans. B*, 1997, vol. 28B, pp. 563–76.
23. E. Jak, P. Hayes, A.D. Pelton, and S.A. Decterov: *Int. J. Mater. Res.*, 2007, vol. 98, pp. 847–54.
24. T. Hidayat, D. Shishin, S.A. Decterov, and E. Jak: *J. Phase Equilib. Diffus.*, 2017, vol. 38, pp. 477–92.
25. T. Kawasaki and H. Ishizuka: *J. Mineral. Petrol. Sci.*, 2008, vol. 103, pp. 255–65.
26. B. Phillips and A. Muan: *J. Am. Ceram. Soc.*, 1958, vol. 41, pp. 445–54.
27. E. Schurmann and G. Kraume: *Arch. Eisenhüttenwes.*, 1976, vol. 47, pp. 435–39.
28. S. A. Decterov, I. H. Jung, E. Jak, Y. B. Kang, P. C. Hayes and A. D. Pelton, In *SAIMM Symposium Series S36 (VII Int. Conf. on Molten Slags, Fluxes & Salts)*, ed. C. Pistorius (The South African Institute of Mining and Metallurgy, Johannesburg, Republic of South Africa: 2004), pp 839–50.
29. T. Hidayat, D. Shishin, S.A. Decterov, and E. Jak: *Metall. Mater. Trans. B*, 2016, vol. 47B, pp. 256–81.
30. S. Cheng, M. Shevchenko, P.C. Hayes, and E. Jak: *Experimental Phase Equilibria Studies in the FeO-Fe<sub>2</sub>O<sub>3</sub>-CaO system, private communication*, The University of Queensland, Brisbane, QLD, PYROSEARCH, 2020.
31. M.D. Burdick, *J. Res. Nat. Bur. Stand., US Dept. of Commerce, Research paper RP1340*, 1940, vol. 25, pp. 475–88.
32. B. Phillips and A. Muan: *J. Am. Ceram. Soc.*, 1959, vol. 42, pp. 413–23.
33. S. Nikolic, H. Henao, P.C. Hayes, and E. Jak: *Metall. Trans. B*, 2008, vol. 39B, pp. 189–99.
34. M.I. Pownceby, J.M.F. Clout and M.J. Fisher-White, *Trans. Inst. Min. Metall., Sect. C*, 1998, vol. 107, pp. C1–C9.
35. M.I. Pownceby and T.R.C. Patrick: *Eur. J. Mineral.*, 2000, vol. 12, pp. 455–68.
36. M. Shevchenko and E. Jak: *Metall. Mater. Trans. B*, 2019, vol. 50B, pp. 2780–93.
37. M. Shevchenko and E. Jak: *Ceram. Int.*, 2019, vol. 45, pp. 6795–6803.
38. T. Hidayat, D. Shishin, S.A. Decterov, and E. Jak: *CALPHAD*, 2016, vol. 56, pp. 58–71.
39. E. Jak, P. C. Hayes and H. G. Lee, *Met. Mater. (Seoul, Repub. Korea)*, 1995, vol. 1, pp. 1–8.
40. E. Jak, In *9th Intl. Conf. on Molten Slags, Fluxes and Salts (MOLTEN12)*, The Chinese Society for Metals: Beijing, China, 2012, p. W077.
41. J. Philibert, *X-Ray Opt. X-Ray Microanal., 3rd Intl. Symp., Stanford Univ.*, 1963, pp. 379–92.
42. P. Duncumb and S.J.B. Reed, Tube Investments Res. Lab., Cambridge, 1968.
43. P. Duncumb, *Electron Microsc. Anal., Proc. Anniv. Meet., 25th*, 1971, pp. 132–37.
44. S. Nikolic, P.C. Hayes, and E. Jak: *Metall. Mater. Trans. B*, 2009, vol. 40B, pp. 892–99.
45. A. Fallah-Mehrjardi, T. Hidayat, P.C. Hayes, and E. Jak: *Metall. Mater. Trans. B*, 2017, vol. 48, pp. 3002–16.
46. T. Kawasaki and H. Ishizuka: *J. Mineral. Petrol. Sci.*, 2008, vol. 103, pp. 255–65.
47. X. Llovet, P.T. Pinard, J.J. Donovan and F. Salvat, *J. Phys. D*, 2012, vol. 45, pp. 225301/1-225301/12.
48. M. Shevchenko and E. Jak: *J. Phase Equilib. Diff.*, 2019, vol. 40, pp. 319–55.
49. M. Shevchenko and E. Jak: *IJMR (International Journal of Materials Research)*, 2019, vol. 110, pp. 600–07.
50. M. Shevchenko and E. Jak: *J. Phase Equilib. Diff.*, 2019, vol. 40, pp. 671–85.
51. M. Shevchenko and E. Jak: *J. Phase Equilib. Diff.*, 2020, vol. 41, pp. 207–17.
52. M. Shevchenko and E. Jak: *Ceram. Int.*, 2019, vol. 45, pp. 6795–6803.
53. M. Shevchenko and E. Jak: *Metall. Mater. Trans. B*, 2018, vol. 50B, pp. 2780–93.
54. M. Shevchenko and E. Jak: *Calphad*, 2020, <https://doi.org/10.1016/j.calphad.2020.101800>.
55. E. Jak, S.A. Decterov, P. C. Hayes and A. D. Pelton, In *Proc. 5th Int. Conf. on Molten Slags, Fluxes and Salts*, (Iron and Steel Soc., AIME, Sydney, Australia: 1997), pp 621–28.
56. S. A. Decterov, I.-H. Jung, E. Jak, Y.-B. Kang, P. Hayes and A. D. Pelton, In *SAIMM Symposium Series S36 (VII Int. Conf. on Molten Slags, Fluxes & Salts)*, ed. C. Pistorius (The South African Institute of Mining and Metallurgy, Johannesburg, Republic of South Africa: 2004), pp 839–50.
57. M. Shevchenko and E. Jak: *Calphad*, 2020, <https://doi.org/10.1016/j.calphad.2020.101807>.

**Publisher's Note** Springer Nature remains neutral with regard to jurisdictional claims in published maps and institutional affiliations.